PERGAMON

Journal of Structural Geology 25 (2003) 1193–1212

JOURNAL OF STRUCTURAL GEOLOGY

www.elsevier.com/locate/jsg

Kinematics of thrust sheets within transverse zones: a structural and paleomagnetic investigation in the Appalachian thrust belt of Georgia and Alabama

Germán Bayona[a,*], William A. Thomas[a], Rob Van der Voo[b]

[a]*Department of Geological Sciences, University of Kentucky, Lexington, KY 40506, USA*
[b]*Department of Geological Sciences, University of Michigan, Ann Arbor, MI 48109, USA*

Received 5 May 2002; received in revised form 12 September 2002; accepted 1 October 2002

Abstract

Deformation styles of orogenic belts change along strike across transverse zones (TZs); hence, the kinematics of TZs is indispensable for three-dimensional restoration of thrust belts. We investigate the causes of deviation in strike of fold axes and fault surfaces in two TZs of the southern Appalachians using structural cross-sections and paleomagnetism. In the Rising Fawn TZ of Georgia, hanging-wall lateral-ramp folds yield paleomagnetic rotations and variation in magnitude of thrust translation. Plunge of folds, differential slip, and rotations are associated with lateral-ramp geometry and along-strike variation in the rheology and thickness of units that host lower and upper detachment levels. In Alabama, the internal geometry, strike, and paleomagnetic rotations of the Helena thrust sheet change across the Anniston TZ. These differences resulted from movement of the Helena thrust sheet over different footwall blocks and sub-décollement basement graben structures, and from differential slip along an oblique ramp. Rotations of thrust sheets within TZs occur where a thrust sheet was translated over: (1) an oblique/lateral ramp with contrasting rock strengths at lower and upper detachment levels, (2) a transverse basement fault that separates contrasting basement structural domains, and (3) intersections between frontal ramps and transverse structures. Because of the local causes of rotations in lateral structures, paleomagnetic and structural analyses of TZs are necessary for understanding the kinematics and restoration of both single thrust sheets and large-scale curves in thrust belts.

Keywords: Thrust-sheet rotation; Transverse zones; Hanging-wall plunging folds; Lateral ramps

1. Introduction

The southern Appalachian foreland thrust belt in Alabama and Georgia consists of late Paleozoic (Alleghanian), large-scale, northeast-striking, northwest-vergent thrust faults and associated folds bounded by undeformed strata on the northwest and by the Talladega slate belt and Appalachian Piedmont on the southeast (Fig. 1). The trace of the southern Appalachian thrust belt defines regional curves around the Tennessee salient and Alabama recess. The regional-scale curves are interrupted by transverse zones (Thomas, 1990), where thrust-belt folds and faults either end or curve abruptly in contrast to the curvilinear regional northeast strike (Fig. 1). Understanding of the geometry and kinematics at lateral terminations of structures is indispensable for three-dimensional analysis and restoration of fold and thrust belts (McCaig and McClelland, 1992; Allerton, 1998). This article reports our investigation of the kinematics, especially thrust sheet rotations, at along-strike terminations of fault-related folds and at an abrupt curve of a thrust sheet.

Lateral terminations, local thrust-sheet rotations, and variations in the amount of shortening of fault-related folds have been attributed to (1) a lateral decrease in magnitude of slip (a displacement gradient) along a frontal ramp, (2) presence of a lateral/oblique ramp, or (3) a combination of a displacement gradient and the presence of a lateral/oblique ramp (Fig. 2) (Apotria, 1995; Allerton, 1998; Wilkerson et al., 2002). Although geometry of the footwall fault surface differs among these models, lateral terminations of fault-related hanging-wall folds may have similar plunge patterns in map view and cross-sections (cross-section A–A′ in Fig. 2) (Wilkerson et al., 2002). The footwall fault-surface geometry

* Corresponding author.
E-mail address: gbayo2@uky.edu (G. Bayona).

0191-8141/03/$ - see front matter © 2003 Elsevier Science Ltd. All rights reserved.
PII: S0191-8141(02)00162-1

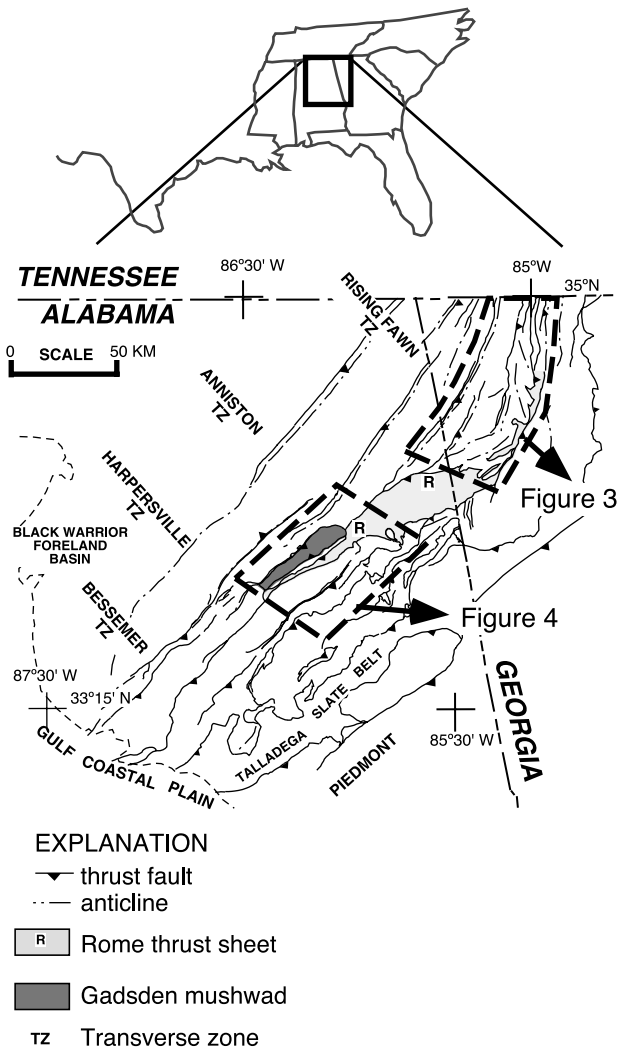

Fig. 1. Structural outline map of Appalachian thrust belt in Alabama and Georgia, showing location of transverse zones (TZ) and study areas (modified from Thomas and Bayona, 2002).

in the model of displacement gradient has only a frontal ramp; in contrast, in the other two models a lateral/oblique ramp in the footwall serves as a cross-strike link between offset segments of a frontal ramp. In all three models, the ramps connect lower and upper stratigraphic levels of detachment. Lateral/oblique ramps are a common characteristic in thrust belts (Boyer and Elliott, 1982), and among the possible causes of locations of lateral/oblique ramps are sub-décollement basement faults, pre-thrusting deformation of cover strata above basement faults, and/or along-strike variations in mechanical stratigraphy (e.g. Thomas, 1990). Cross-strike alignments of lateral/oblique ramps, transverse faults, and displacement-transfer zones comprise transverse zones in thrust belts (Thomas, 1990).

Identification of lateral/oblique ramps in a thrust belt is indispensable because hanging-wall strata and pre-existing structures (e.g. cleavage, fractures, lineaments) are extended or shortened, and such structures together with paleocurrent directional indicators may be rotated with respect to regional orientations (e.g. Apotria et al., 1992; Wilkerson et al., 1992). Wilkerson et al. (2002) evaluated separately each of the following criteria to determine whether a plunging hanging-wall fold is related to a displacement gradient at a frontal ramp, to a lateral/oblique ramp, or a combination of both mechanisms: (1) angle of plunge of hanging-wall strata, (2) angle between hanging-wall cut-off lines and fault strike, (3) angle between strike of hanging-wall stratigraphic contacts and fault strike, (4) stratigraphic separation diagrams, and (5) abrupt change in strike of a fault. Other criteria from cross-sections and geologic maps may be used to identify the mechanism of lateral terminations of fault-related folds. At an oblique/lateral ramp and in the direction down plunge of hanging-wall strata, translation of hanging-wall strata continues along-strike but at an upper level of detachment. In the displacement-gradient model, translation decreases down-plunge of hanging-wall structures toward the lateral termination of the fault (Fig. 2). Identification of a footwall lateral ramp in map view is indicated by drape of hanging-wall beds and the thrust-fault surface over footwall lateral cutoffs (cross-section B–B′ in Fig. 2) (Thomas, 1990). In a three-dimensional restoration, the footwall lateral cut-off must match the equivalent hanging-wall lateral cut-off (e.g. Thomas and Bayona, 2002). A fundamental characteristic of lateral/oblique ramps is the contrast in lithology between units that host lower and upper levels of detachment, and the ramp. We apply various structural criteria and paleomagnetism techniques to determine the mechanisms that caused the lateral termination and deviation in strike of plunging of folds in the composite Clinchport–Horseleg thrust sheet in Georgia, as well as the abrupt change in strike of the Helena thrust sheet in Alabama (Figs. 1, 3, and 4).

Paleomagnetic studies considering the regional kinematics of thrust belts have emphasized that knowledge of the pre-existing configuration of foreland basement uplifts and continental margins, as well as genetically related variations in stratigraphy, is essential for the understanding of the geometry of the thrust belt. Paleomagnetic investigations of the central and southern Appalachians (e.g. Schwartz and Van der Voo, 1983; Kent, 1988; Stamatakos and Hirt, 1994; Stamatakos et al., 1996) and tectonostratigraphic studies (Rankin, 1976; Thomas, 1977) have concluded that the curvature of the central and southern Appalachians was inherited from the older rifted continental margin of Laurentia. Studies in the Wyoming–Idaho and Sevier thrust belts have documented curvature in response to either the buttressing effects of uplifted basement-cored blocks within the foreland or to differential propagation caused by along-strike variations in pre-deformational basin geometry, or possibly both (Grubbs and Van der Voo, 1976; Schwartz and Van der Voo, 1984; Eldredge and Van der Voo, 1988; Montgomery, 1993; Paulsen and Marshak, 1999). In the Appalachian thrust belt in Alabama, different types of thin-skinned transverse structures evolved in response to a transverse basement fault and differences in

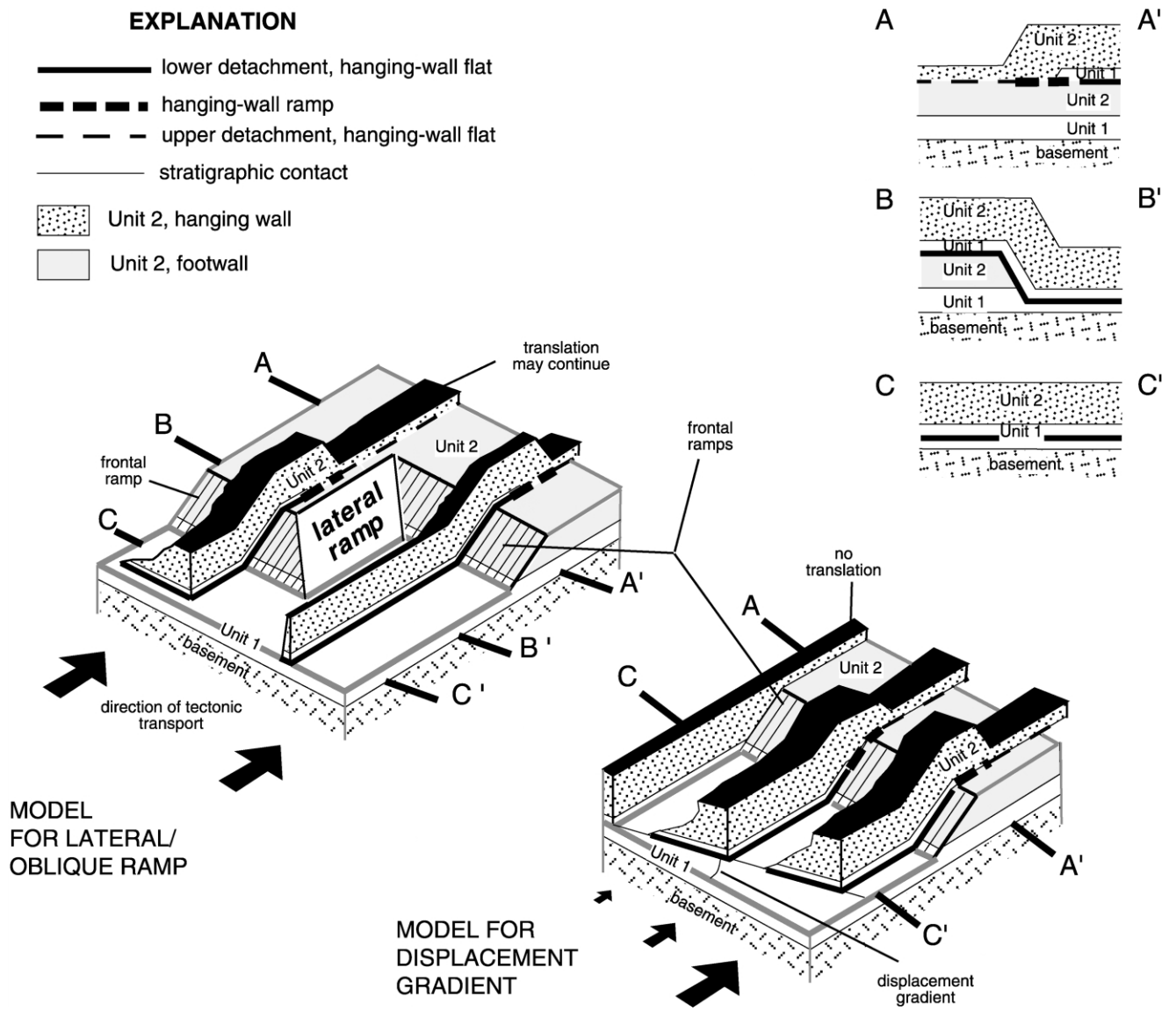

Fig. 2. Schematic block diagrams and strike-parallel cross-sections, showing two possible mechanisms to explain the lateral termination and plunging of hanging-wall strata. Cross-sections A–A′ and C–C′ apply to both models, whereas cross-section B–B′ only applies for the model of lateral/oblique ramp. A third mechanism is a combination of a lateral/oblique ramp (left) and displacement gradient (right) mechanisms (see fig. 8d of Wilkerson et al., 2002).

elevation of the top of basement (Thomas and Bayona, 2002). However, it is not clear whether locations of transverse structures in the thrust belt in Georgia are also influenced by relief of the top of basement and location of basement transverse faults.

Published paleomagnetic data from Ordovician and Silurian clastic rocks in the southern Appalachians indicate that paleomagnetic techniques may be useful to constrain vertical-axis rotations of thrust sheets. Watts and Van der Voo (1979) and Morrison and Ellwood (1986) documented at least two components of magnetization in Ordovician rocks with directions, after correction for the tilt of the strata, that are west-northwest/upward and south-southeast/downward. Positive fold(tilt)-tests have been obtained for the west-northwest/upward component of the Upper Ordovician Moccasin-Bays Formations (Watts and Van der Voo, 1979). The well-defined south-southeast/downward magnetization component documented in the Silurian Red Mountain Formation in Alabama (Perroud and Van der Voo, 1984; Hodych et al., 1985) has been associated with a late Paleozoic remagnetization that also affected other Appalachian strata; however, time of folding relative to time of remagnetization varies across and along the strike of the Appalachian thrust belt (Stamatakos et al., 1996). The remanent magnetization in all these studies is chemical and carried dominantly by hematite (Watts and Van der Voo, 1979; Perroud and Van der Voo, 1984; Hodych et al., 1985; Morrison and Ellwood, 1986).

Because a pre-folding component of magnetization is a requisite for the analysis of thrust sheet rotations, we

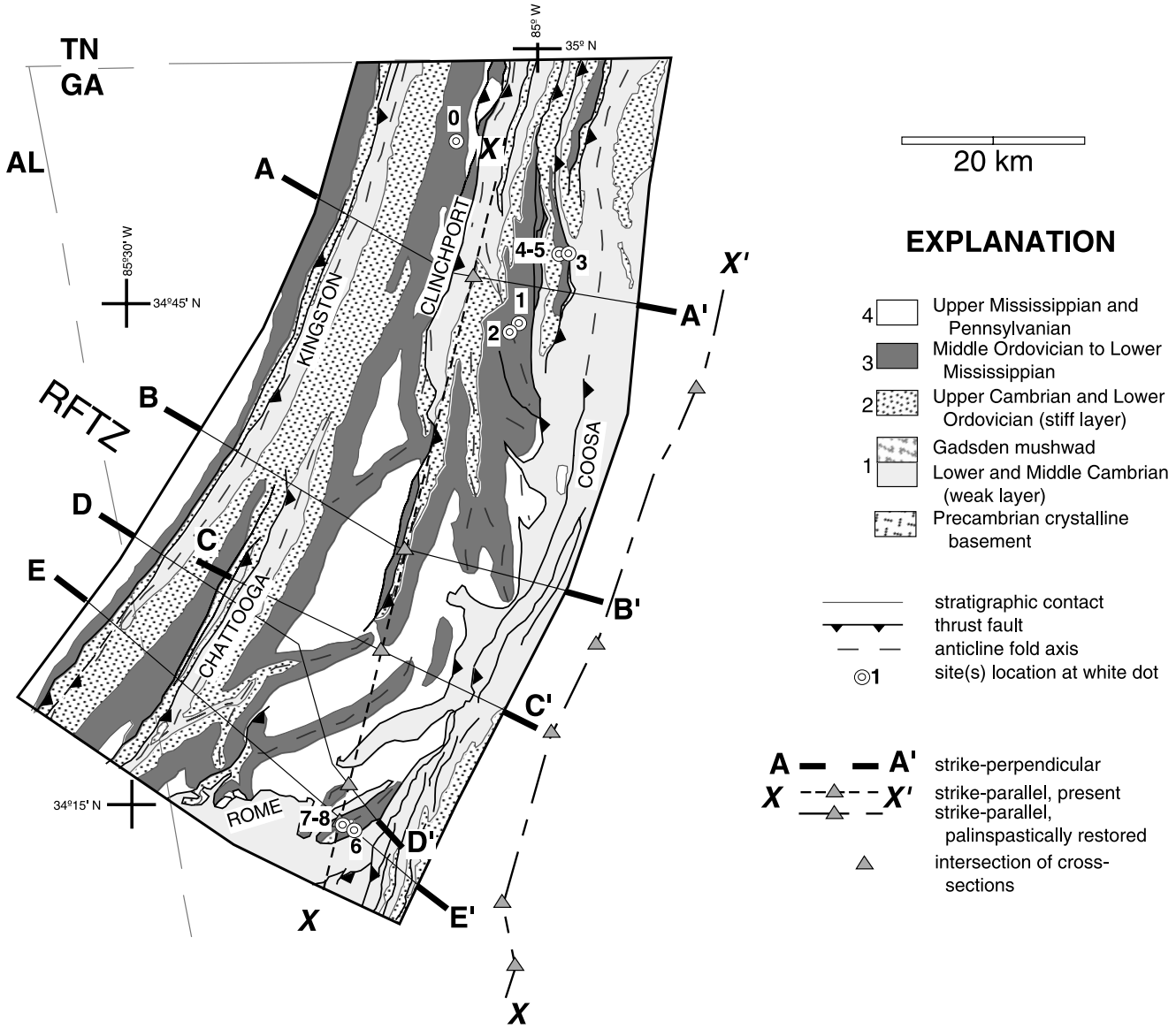

Fig. 3. Geologic map of the composite Clinchport–Horseleg thrust sheet in Georgia (upper page) (modified from Cressler (1974) and Chowns and Carter (1983)) and four representative structural cross-sections (lower page). Faults are labeled in capital letters. Abbreviation: RFTZ = Rising Fawn transverse zone. Site 0 is from Morrison and Ellwood (1986), sites 1 and 2 are in the Dalton area, sites 3–5 are in the Hamilton Mountain area, and sites 6–8 are in the Horseleg Mountain area. Three strike-perpendicular cross-sections (A–A′, B–B′, and E–E′) are shown here and (along with C–C′ and D–D′, not shown) are the basis for construction of strike-parallel cross-section X–X′. Intersection points between cross-sections at the top of unit 2 are restored to palinspastic positions and used to delineate the shape of line X–X′ in palinspastically restored position. Horizontal linear distances between corresponding present and restored locations of intersection points are plotted as the translation distances in Fig. 10c. The cross-sections are based on outcrop geology and six seismic reflection profiles.

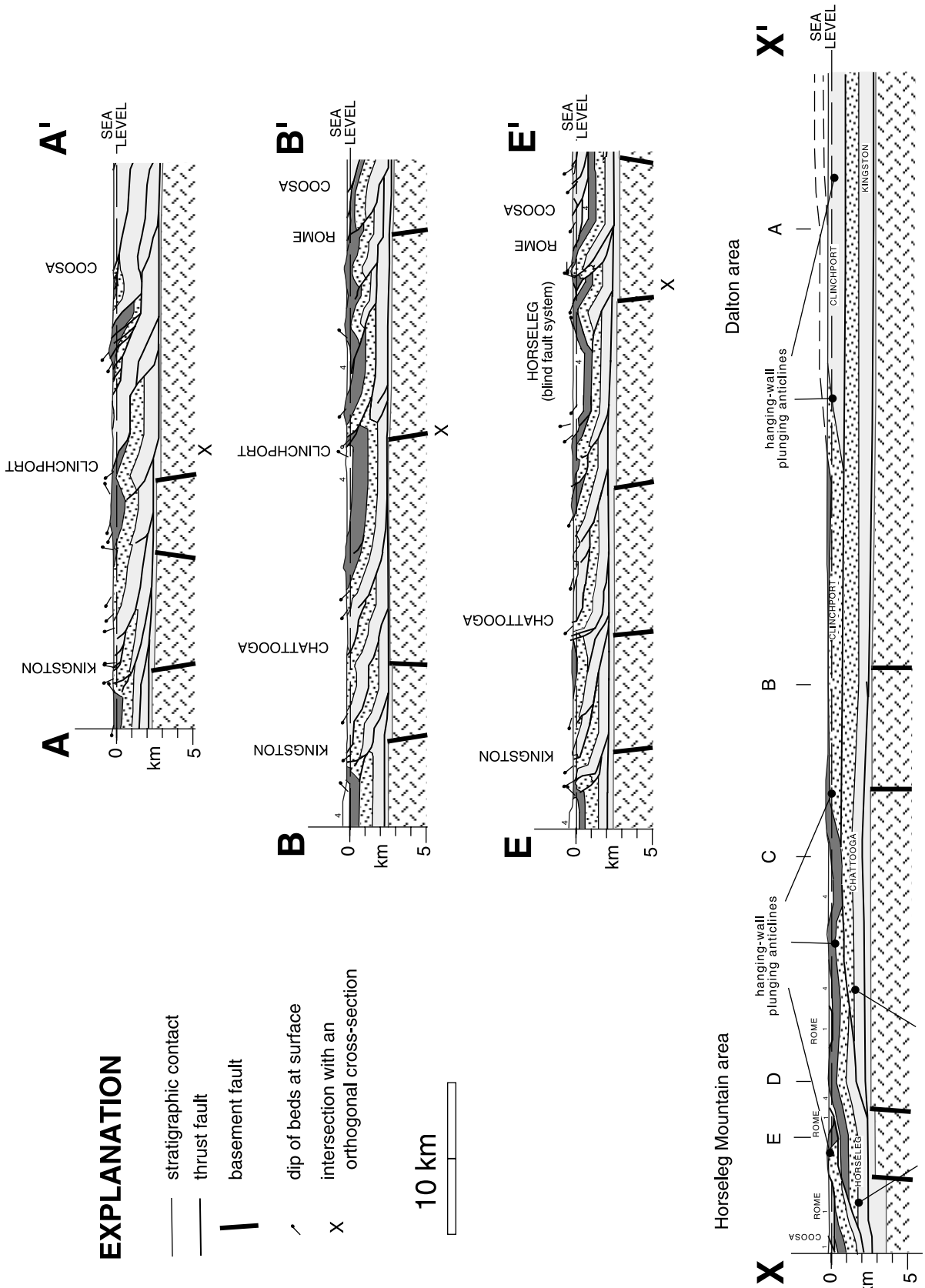

Fig. 3 (*continued*)

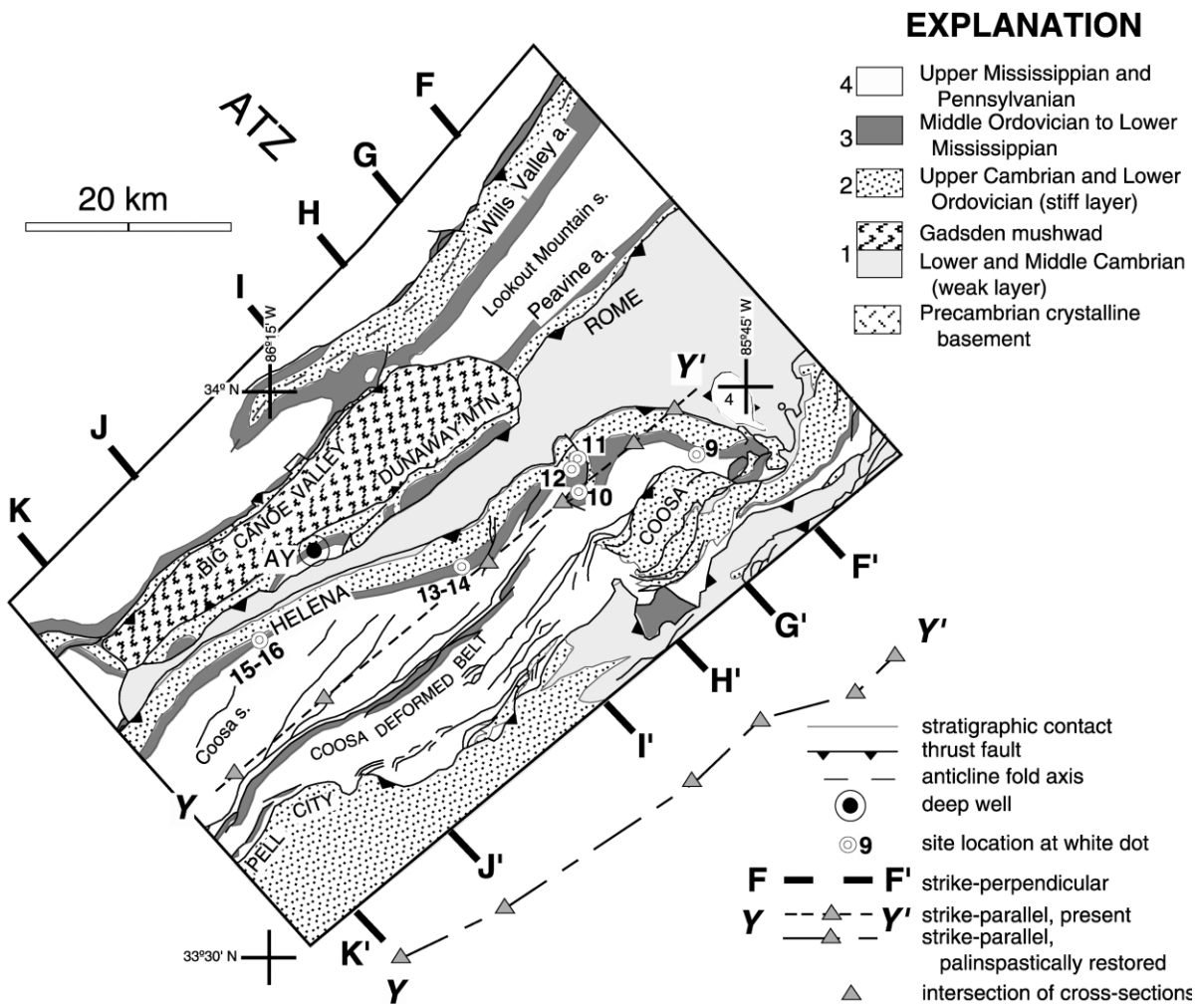

Fig. 4. Geologic map of the study area in the Helena thrust sheet (left page) (modified from Osborne et al., 1988) and four representative structural cross-sections (right page). Faults are labeled in capital letters; folds are in capital and lower case (a = anticline; s = syncline/synclinorium). Abbreviations: MTN = Mountain; ATZ = Anniston transverse zone. Stratigraphic units 3 and 4 are not differentiated in the thin imbricate thrust sheets in the Coosa deformed belt. Site 9 is in the northeastern segment of the Helena thrust sheet, sites 10–12 are near the transverse fault, and sites 13–16 are in the southwestern segment of the Helena thrust sheet. Three strike-perpendicular cross-sections (G–G′, I–I′, and J–J′) are shown here and (along with F–F′, H–H′, and K–K′, not shown) are the basis for construction of strike-parallel cross-section Y–Y′. Intersection points between cross-sections at the top of unit 1 are restored to palinspastic positions and used to delineate the shape of line Y–Y′ in palinspastically restored position. The cross-sections are based on outcrop geology, seven seismic reflection profiles, and one deep well (AY—Amoco No. 1 Young, section 34, T 13 S, R 4 E, St. Clair County).

initially conducted a paleomagnetic sampling in the Upper Ordovician Greensport and Sequatchie Formations in Alabama in order to establish areas and units in which an Ordovician component of magnetization could be isolated. These units consist of red shales and siltstones with thin interbeds of fine-grained sandstones; the clastic facies pinches out gradually northwestward into a dominantly carbonate succession (Drahovzal and Neathery, 1971; Carter and Chowns, 1986). The Ordovician and late Paleozoic directions of magnetization reported previously in the southern Appalachians were isolated in cores from the lower red, fine-grained sandstones and sandy siltstones of the Greensport Formation. These beds crop out in our study areas, and they were the target unit for paleomagnetic sampling of this study.

2. Methods

Construction of strike-perpendicular and strike-parallel cross-sections, as well as a map of the top of basement, is constrained by surface and subsurface data. Balancing of strike-perpendicular cross-sections and palinspastic restoration of thrust sheets are explained in Thomas (2001) and Thomas and Bayona (2002).

A total of 140 paleomagnetic cores, collected at sites numbered 1 to 16 in Figs. 3 and 4, were analyzed for this study. 130 oriented cores were collected using a portable drill and a magnetic compass at sites 1–16, and the remaining 10 cores were obtained from three oriented hand samples collected in sites 13, 14, and 16. Site distribution was designed to permit the application of a fold(tilt) test to

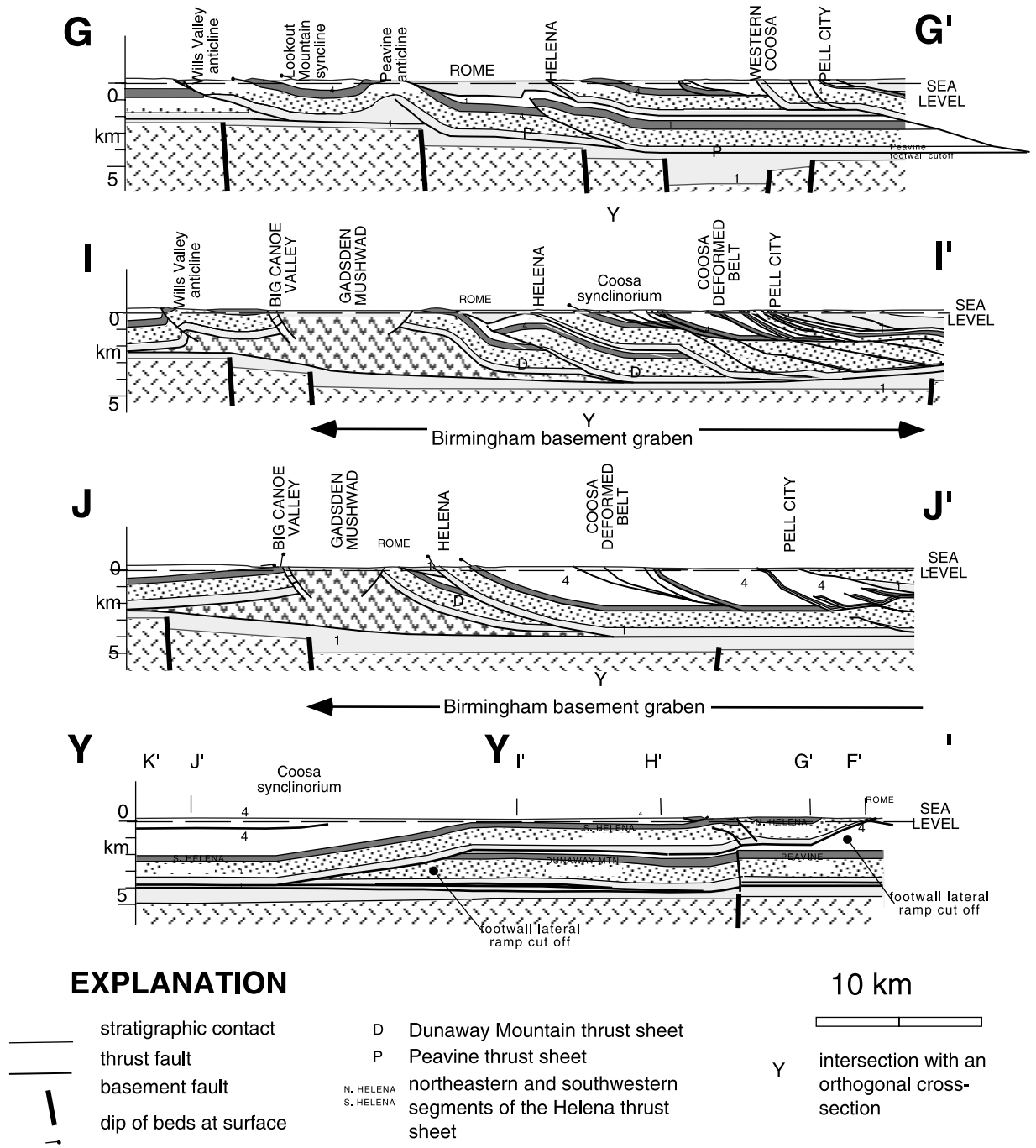

Fig. 4 (*continued*)

assess the likelihood of the magnetization being representative of the Ordovician geomagnetic field and to determine whether rotations had affected different strike domains of the Helena thrust sheet and of plunging folds in Georgia. The scatter and scarcity of exposures of the Greensport Formation, intense outcrop weathering, and significant deformation limited selection of sites. The Upper Ordovician Greensport Formation was sampled at sites 2–16, and the Upper Ordovician Sequatchie Formation was sampled at site 1. Standard 2.4 cm diameter cores with 2.2 cm height were progressively demagnetized in an Analytical Service Co. (ASC) thermal demagnetizer, and natural remanent magnetization (NRM) was measured with a three-axis cryogenic 2G magnetometer in the field-free room at the University of Michigan. All of the specimens were subjected to thermal demagnetization with cooling to room temperature in zero magnetic field. Increments of thermal demagnetization were <50 °C from 300 to 500 °C, <30 °C from 500 to 600 °C, and <20 °C from 600 to 680 °C in an attempt to resolve intermediate- and high-temperature components of NRM for each core. Components of magnetization were calculated from Principal

Component Analysis interpreted with the aid of orthogonal demagnetization diagrams (Zijderveld, 1967). We used the IAPD2000 software of the Geological Survey of Norway to run all the paleomagnetic calculations of this study.

Mean magnetization directions were calculated using Fisher's statistics (Fisher, 1953), giving unit weight to field- or laboratory-drilled cores. Local incremental fold(tilt) tests were used to determine the timing of magnetization with respect to deformation. Because of local rotations, incremental inclination-only tilt tests (McFadden and Reid, 1982) allow accounting for the statistically significant clustering of inclinations at different steps of unfolding. The significance of the fold(tilt) test followed the criteria of McElhinny (1964) because of the limited number of sites per limb. Corrections for plunge were not made because of the limited number of sites and the very low angle of plunge ($<5°$) in folds that yielded a positive test. Upon establishing the approximate age of magnetization, a reference declination was calculated from the Paleozoic apparent polar wander path of Laurentia in order to estimate the magnitude and relative sense of rotations. Even with the limited sampling distribution, comparisons of mean paleomagnetic directions of structural domains within each area allow a statistical documentation of the significance of local thrust-sheet rotations.

3. Structure of the thrust belt and basement

3.1. Lithotectonic units

Appalachian thrust-belt structures encompass a Paleozoic succession spanning Cambrian to Pennsylvanian strata. For cross-section construction, Paleozoic strata are divided into four units: a basal weak unit (mostly Rome and Conasauga Formations, unit 1), a regionally dominant stiff layer (Knox Group, unit 2), a heterogeneous carbonate–siliciclastic Middle Ordovician–Lower Mississippian succession (unit 3; this unit includes the Greensport–Sequatchie Formations), and Upper Mississippian–Pennsylvanian synorogenic foreland deposits (unit 4). The regional décollement is within the basal weak unit above Precambrian crystalline basement (e.g. Thomas, 1985; Thomas and Bayona, 2001).

3.2. Regional structure, configuration of the top of basement, and timing of deformation

Along- and across-strike changes in thrust belt geometry are closely related to basement structural relief beneath the thrust belt (Fig. 5) (Bayona, 2003). The northwestern (frontal) part of the thrust belt is dominated by broad, flat-bottomed synclines and large-scale, northeast-trending, asymmetric anticlines. Structures immediately southeast of the frontal fault-related folds exhibit dramatic changes both along- and across-strike at transverse zones (Thomas and Bayona, 2001). Top of basement beneath the leading imbricate faults is shallow and flat, but it abruptly drops southeastward across basement faults into the deep Birmingham graben, a subsurface structure documented by seismic reflection profiles (e.g. cross-section I–I′ in Fig. 4). In Alabama, the depth of the regional décollement, as well as the amplitude of thrust ramps, increases abruptly southeast of the Big Canoe Valley fault and Peavine anticline (Fig. 4), which are positioned over the down-to-southeast boundary fault system of the Birmingham graben. Tectonic thickening of graben-fill strata controls deformation southwest of the Anniston transverse zone (Gadsden mushwad in Figs. 1 and 4) (Thomas, 2001), whereas ramp-and-flat geometry of the thrust belt dominates northeast of the Anniston transverse zone. Shallow imbricate faults dominate the thrust belt in Georgia, where the top of basement dips gently but irregularly southeastward. Plunging folds in intermediate imbricate faults have irregular orientations that contrast with the straight, northeasterly strike of leading imbricate faults (Fig. 3). Southeastern trailing thrust sheets consist of duplexes that involve units 1 and 2.

Along-strike changes of the structural configuration of the top of basement are concentrated at northwest-striking basement faults, which offset northeast-striking basement faults (Fig. 5). Transverse zones of the overlying thin-skinned thrust belt geographically coincide with the offsets of northeast-striking basement faults (Figs. 1, 3, and 4). Tectonostratigraphic analyses in a palinspastic map of Lower and Middle Cambrian strata indicate a complex distribution of rift-related deposits across these northwest- and northeast-striking basement faults (Thomas et al., 2000; Bayona and Thomas, 2001).

The foreland thrust belt of Alabama and Georgia records both forward and out-of-sequence thrusting (e.g. Thomas, 2001). Geologic map patterns of the trace of the Rome thrust sheet (R in Fig. 1), a flat and shallow structure, indicate at least two events of deformation along the Horseleg fault system, and an out-of-sequence break-back of the Helena thrust sheet. In Georgia, the Rome thrust fault truncates folds in the footwall, and the fault surface is folded coaxially by the footwall folds (e.g. labels for sites 6–8 in Fig. 3) (Cressler, 1970). Truncations of southeast-dipping strata and local structures by the Rome thrust fault also are mapped in Alabama, northwest of the Helena thrust sheet (Dunaway Mountain and Peavine anticline; Fig. 4) (Osborne et al., 1988; Garry, 2001). These observations suggest an event of folding prior to the emplacement of the Rome thrust sheet; subsequent folding tightened the Rome footwall folds and folded the Rome thrust sheet in Georgia. In Alabama, translation of the Helena thrust sheet broke upward through the trailing part of the Rome thrust sheet, disconnecting it from hinterland thrust sheets (Thomas, 2001; Thomas and Bayona, 2002).

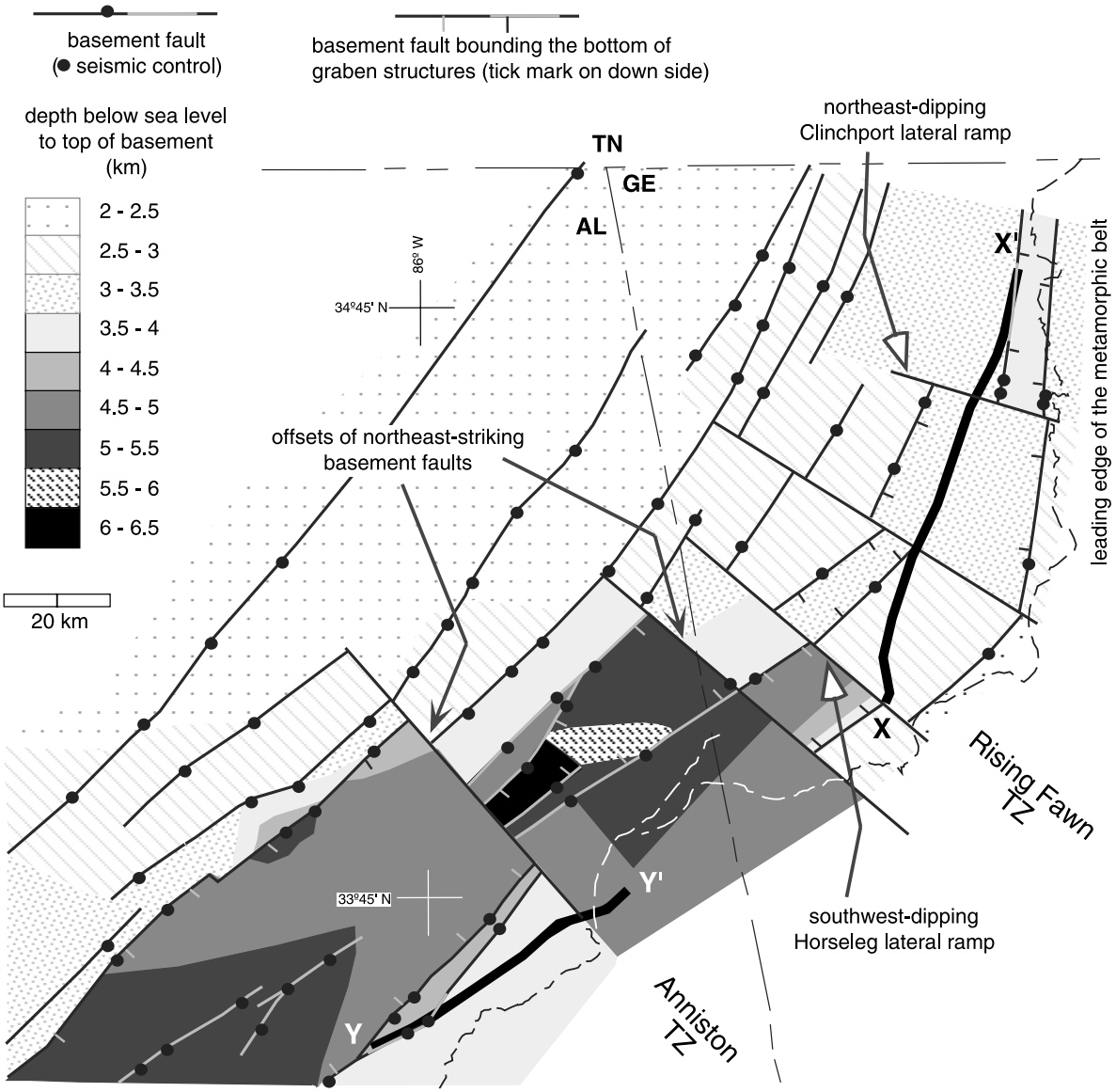

Fig. 5. Map of depth below sea level to the top of basement, showing traces of subdetachment basement faults, structural relief of the Birmingham graben, and relationship between position of transverse basement faults and transverse zones (TZ) in the thin-skinned foreland thrust belt. The northeastern segment of the Helena thrust sheet restores northeast of the Anniston transverse zone. Note contrasting geometry of the Birmingham graben on opposite sides of the Anniston transverse zone and offsets of the northeast-striking basement fault system at transverse zones. Lines X–X′ and Y–Y′ (from Figs. 3 and 4, respectively) are in palinspastic position. Locations of Clinchport and Horseleg lateral ramps along line X–X′ correspond to changes in elevation of top of basement across transverse basement faults. Line Y–Y′ restores near the southeastern shoulder of the Birmingham graben.

4. Structure of the Clinchport–Horseleg composite thrust sheet and location of sites

Several strike domains of folds and faults have been mapped between the northeast-striking Kingston fault and the Rome–Coosa faults in Georgia (Fig. 3) (Cressler, 1974; Chowns and Carter, 1983; Coleman, 1988). From north to south, the Clinchport fault cuts up section from a thick unit 1 to a thin unit 1 and, farther south, to the base of the stiff unit 2, forming two south-plunging hanging-wall ramp anticlines. Two south-southeast-plunging, asymmetrical anticlines (sites 1 and 2 are in the northern anticline; Fig. 3) diverge from the south-southwest-striking Clinchport fault between the two ramp anticlines (Cressler, 1974). The Clinchport fault extends southward at the base of the stiff layer (upper-level detachment) and ends in a south-southwest-plunging fold. A north-striking, asymmetrical anticline and syncline (sites 3–5 in the syncline; Fig. 3) are in a trailing imbricate thrust sheet. South of the south end of the Clinchport fault, east-northeast-plunging folds diverge from the northeast-striking Chattooga fault within the Rising Fawn transverse zone (Fig. 3). Detailed mapping indicates that the folds plunge into the transverse zone (Coleman, 1988). These asymmetrical folds are the surface expression of the blind Horseleg fault system. The Chattooga and Horseleg faults are detached within unit 1, and the Horseleg

fault cuts up section along strike, in a short distance from south to north, to upper detachment levels within units 2 and 3. Sites 6–8 are located in the easternmost of the east-northeast-plunging asymmetrical folds.

A strike-parallel cross-section illustrates lateral changes in detachment levels and the geometry of hanging-wall and footwall lateral ramps (cross-section X–X′ in Fig. 3). The northeastern end of cross-section X–X′ shows the plunge of two hanging-wall anticlines above a flat fault surface (Clinchport fault) and the southward up-section rise of detachment level from unit 1 (weak unit) to the base of stiff unit 2. The southwestern end of cross-section X–X′ shows high-angle, south-dipping faults (Horseleg fault system) with three hanging-wall plunging anticlines and an abrupt southwestward deepening of the top of basement. Palinspastic geometry of line X–X′ is concave-to-the-hinterland and asymmetrical, suggesting more shortening toward the extremes of the Clinchport–Horseleg thrust sheet and less shortening near the center (at cross-section C–C′ in Fig. 3).

5. Structure of the Helena thrust sheet and location of sites

The Helena thrust fault is characterized by a large-scale curve across a transverse fault, which divides the Helena thrust sheet (HTS) into northeastern and southwestern segments (Fig. 4) (Thomas and Bayona, 2002). The Helena fault in the southwestern segment has an irregular northeasterly strike (sites 13–16 in Fig. 4). Within the Anniston transverse zone (ATZ), interference folds and accommodation faults are in the southwestern segment (sites 11 and 12 are in opposite limbs of the syncline in Fig. 4), and strata in the northeastern segment form an anticline associated with the transverse fault (site 10 in Fig. 4). Eastward across the ATZ, the Helena fault bends gradually to an eastward strike, and the Helena thrust sheet is truncated on the east by the Coosa fault (Graham, 1999). The basal detachment in the northeastern segment cuts up section eastward along strike from unit 1 into the basal part of unit 2 (east of site 9 in Fig. 4). Along the east-striking fault, beds in the Helena hanging wall dip southward, forming the shallower of two down-to-southwest plunging steps that account for ~4000 m of relief in the deep Coosa synclinorium in the HTS. The transverse fault in the HTS is aligned with a sub-décollement transverse basement fault that divides the Birmingham basement graben into a narrow graben on the northeast from a wider and southwest-deepening graben on the southwest (Fig. 5) (Thomas and Bayona, 2002).

The strike-parallel cross-section Y–Y′ illustrates geometry of footwall lateral ramps and the location of transverse faults (Fig. 4). The two down-to-southwest plunging steps of the Helena thrust sheet follow the geometry of two southwest-dipping footwall lateral ramps, which are within two different footwall thrust sheets (Dunaway and Peavine) and at different stratigraphic levels. The stratigraphic level of detachment is generally within unit 1 and persists southwestward along strike, indicating that draping over footwall lateral ramps causes the plunge in the hanging-wall beds. The trend of line Y–Y′ in palinspastic position indicates a northeastward increase of shortening with an abrupt increase eastward across the transverse basement fault.

Subsurface mapping beneath the Helena thrust sheet indicates abrupt changes of elevations of top of basement and footwall deformation across the ATZ (Figs. 4 and 5) (Thomas and Bayona, 2002). Footwall thrust sheets in the foreland of the southwestern segment of the HTS and southwest of the ATZ are deformed and dip northwestward within the wide Birmingham graben. In contrast, a nearly undeformed footwall thrust sheet overlies a generally shallower and narrower graben northeast of the ATZ. The northeastern segment of the HTS is deformed according to a ramp-flat-ramp configuration of the corresponding footwall.

6. Paleomagnetic results

6.1. The multivectorial magnetization

Thermal demagnetization of Greensport Formation cores uncovered all three magnetic components previously isolated in red Ordovician clastic rocks of the southern Appalachians (Fig. 6). A low-temperature (A) component has a direction parallel to the present Earth's field with unblocking temperatures <300 °C; a secondary (B) component has unblocking temperatures from 400 to 590 °C; a characteristic (C) component has persistent directions at temperatures >590 °C and unblocking temperatures up to 680 °C. The A and B magnetic components were isolated in the Sequatchie Formation (Fig. 6i); however, the cores (except one) do not decay uniformly to the origin, suggesting the presence of an unresolved high blocking-temperature component. The C component was isolated in cores from all 16 sites; however, the C component was uncovered in less than three cores of the total of the demagnetized cores from sites 1, 4, 5, and 14–16. The B component was isolated in cores from 15 sites; however, four sites 3, 9, 10, and 12 have only one core with component B. Resulting site-mean directions are listed in Table 1.

6.2. The characteristic C component

The C component has a dominant west-to-northwest and up (C1) direction, but east-to-southeast and down (C2) directions were isolated in sites 1, 5, and 11 (one core per site; Table 1). Incremental unfolding in Horseleg Mountain (sites 6 and 7) and Glencoe areas (sites 11 and 12) yields a significant positive fold(tilt) test for the C1 component (Fig. 7a and b). In Hamilton Mountain (sites 3–5), the maximum clustering of inclination data is reached at 100% of

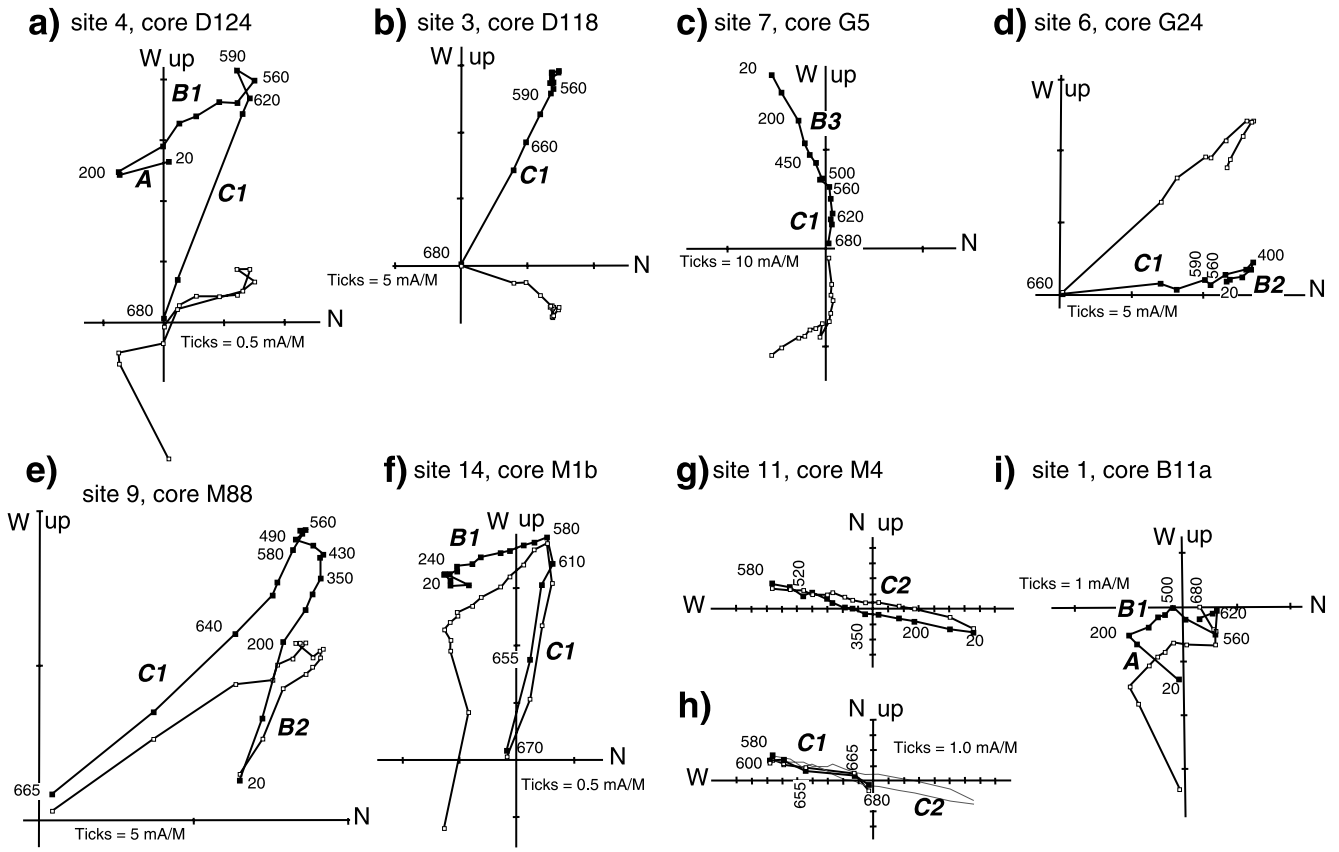

Fig. 6. Representative Zijderveld (1967) diagrams of magnetic components before tilt correction; open and solid squares are vector end points in the vertical and horizontal planes, respectively, and adjacent numbers are temperature in °C. Diagrams (a)–(h) are from cores of the Greensport Formation and diagram (i) is from a core of the Sequatchie Formation. Demagnetization of core M4 (Glencoe area, near the transverse fault) is shown in two diagrams ((g) and (h)) to illustrate the antiparallel directions of C2 and C1 components. Components A, B1, B2, B3, C1, and C2 are labeled along the appropriate segments in the demagnetization diagrams. Component C1, which is used for analysis of rotations after tilt correction, is isolated in demagnetization diagrams (a)–(f) and (h).

unfolding, but the test is not significant at 95% of confidence. In equal area projections, site-mean directions for the C1 component show a good clustering of upward and shallow inclinations after correction for the tilt of strata and an ellipsoidal distribution of the declinations in the northwest quadrant (Fig. 8a and b). The tilt-corrected mean direction of all the sites for the C1 component (296°/ − 19.6°, $k = 26.5$, $\alpha_{95} = 7.9°$) is similar to the directions reported by Morrison and Ellwood (1986) for Ordovician beds in Georgia (Sequatchie Formation, 310°/ − 25°, $k = 93.5$, $\alpha_{95} = 8°$) and by Watts and Van der Voo (1979) for Ordovician red beds in Tennessee (Bays Formation 310°/ − 10°, $k = 62.2$, $\alpha_{95} = 9.8°$; Moccasin Formation 321°/ − 11°, $k = 42$, $\alpha_{95} = 4.5°$). Paleomagnetic directions from sites 7 and 8, which are located on the steeply dipping (more than 70°) northwest flank of the Horseleg Mountain anticline, are used only for the fold(tilt)-test. High degree of internal strain and out-of-plane deformation in steeply dipping strata (e.g. Stamatakos and Kodama, 1991a,b; Apotria et al., 1992) may cause distortion of magnetization vectors.

The C2 component in demagnetization diagrams shows an antiparallel direction with respect to the C1 direction (e.g. Fig. 6g), and directions for the C2 component have a greater cluster after tilt correction. We tentatively interpret C2 as of reversed polarity with respect to the characteristic normal-polarity C1 component, in view of the Laurentian apparent polar wander path. Because the C2 directions are so few in number (one core per site; Table 1), they have not been used in our analysis of rotations.

6.3. The B component

Sites with intermediate blocking-temperature components are divided into three groups, which yield directions B1, B2, and B3. For the B1 component, site-mean directions before tilt correction are to the south-to-southeast and with moderate downward inclinations (Fig. 8c). The mean B1 direction after tilt correction shallows, but the site means spread out in the southern hemisphere (Fig. 8d). Fold(tilt) tests of the B1 component thus indicate a post-folding age of magnetization (Fig. 7c). The mean direction of the B1 component before tilt correction is 150.1°/29.8°, $k = 41.3$, $\alpha_{95} = 6.8°$. The B2 component was isolated in sites 6 and 9

Table 1
Components of magnetization uncovered from the Greensport Formation (sites 2–16), Sequatchie Formation (site 1), and Sequatchie and lowermost Red Mountain Formations (site 0; Morrison and Ellwood, 1986). *N*/*No* = Number of cores used in the analysis/number of cores demagnetized; *DD*°/*D*° = bedding azimuth of dip and dip angle at the site; *D*°/*I*° = site-mean declination/inclination; k/α_{95}° = the Fisher (1953) precision parameter/half-angle of 95% confidence about the mean for sites $N > 2$. Ranges of low and high are temperatures at which the component becomes persistent and its maximum unblocking temperature, respectively. Sites with cores from oriented hand samples and cores drilled in the field are: site 13 (four cores from two hand samples, six cores drilled in the field); site 14 (two cores from one hand sample, seven cores drilled in the field); and site 16 (four cores from one hand sample, three cores drilled in the field)

	Site	*N*/*No*	*DD*°/*D*°	In situ		Tilt corrected		*k*	α_{95}°	Temperatures (°C)	
				D°	*I*°	*D*°	*I*°			Low	High
	C1 component (pre-folding)										
0	Ringgold gap	24/27		314.7	−40.3	310.2	−25.3	93.5	8	>500	650–700
2	C (Dalton)	7/9	235/57	274.4	31.5	269.2	−15.5	22.7	12.9	590–640	680
3	Deast (Hamilton Mtn)	10/11	289/37	296	20.2	295.8	−16.5	17.1	12	450–560	680
4	Dwest1 (Hamilton Mtn)	2/7	96/16	292.9	−26.8	291.3	−11.4	–	–	590	680
6	Geast (Horseleg Mtn)	12/12	144/34	324.2	−54	324.1	−20	36.4	7.3	300–640	680
7	Gwest1 (Horseleg Mtn)	4/5	320/78	281.7	64.6	304.4	−8.1	79.9	10.3	590–640	680
8	Gwest2 (Horseleg Mtn)	4/4	319/70	287.7	40.5	293.6	−22.8	87.9	9.9	560–620	680
9	Canon gap (N. Helena)	10/12	205/32	305.8	−30.5	320.6	−20.2	156.4	3.9	430–560	680
10	Alexander gap	6/7	201/42	269	−17.7	287	−27.7	34.6	11.5	460–620	680
11	E. Glencoe	10/10	194/33	286.7	−15.1	294.6	−11.2	166.8	3.8	580–640	680
12	W. Glencoe	11/11	70/43	303.9	−49.3	283.4	−17	86.6	4.9	490–600	680
13	Greensport gap1	6/10	163/27	301.6	−33.5	308.7	−12	32.6	11.9	490–580	680
14	Greensport gap2	3/9	170/16	279.9	−43.6	292.1	−36.5	210.5	8.5	600–610	680
15	US231 gap-1	1/9	139/20	274.6	−43.6	284	−28.1	–	–	430	680
16	US231 gap-2	3/7	145/24	286.8	−39.8	294.7	−19.8	1265.3	3.5	430	680
	C2 component (pre-folding)										
1	B (Dalton)	1/14	105/35	119.2	31	117.2	−3.2	–	–	560	680
5	Dwest2 (Hamilton Mtn)	1/3	109/24	117.5	17.2	117.2	−6.5	–	–	620	680
11	E. Glencoe	1/10	194/33	103.9	10.1	109.5	8.5	–	–	20	580
	B1 component (first group; post-folding)										
1	B (Dalton)	8/14	105/35	148.8	39.3	138.1	11.4	87.6	6	100–300	500–590
2	C (Dalton)	4/9	235/57	149.6	23.9	167.6	9.2	22.8	19.7	300	560–590
3	Deast (Hamilton Mtn)	1/11	289/37	144.6	46.9	198.3	66.5	–	–	400	560
4	Dwest1 (Hamilton Mtn)	6/7	96/16	142	23.3	138.5	11.8	58.5	8.8	100–200	500–590
5	Dwest2 (Hamilton Mtn)	2/3	109/24	143.6	20.7	141.1	0.5	–	–	200–300	560–590
9	Canon gap (N. Helena)	1/12	205/32	143.3	20.1	149.1	3.2	–	–	400	560
10	Alexander gap	1/7	201/42	170	15.2	168.9	−21	–	–	300	580
12	W. Glencoe	1/11	70/43	134.7	37.4	117.3	12.2	–	–	250	400
13	Greensport gap1	4/10	163/27	151.2	27.5	152.5	1	57.3	12.2	200–300	430–580
14	Greensport gap2	8/9	170/16	157.8	31	159.2	15.3	116.8	5.1	200–300	490–580
15	US231 gap-1	8/9	139/20	154	30.4	152.1	11	181.2	4.1	200–350	460–560
16	US231 gap-2	4/7	145/24	160.4	38.6	157.4	15.3	333.9	5	340	530–560
	B2 component (second group; pre-folding?)										
6	Geast (Horseleg Mtn)	8/12	144/34	132.6	56.8	137.2	23.2	20.1	12.7	20–200	300–400
9	Canon gap (N. Helena)	3/12	205/32	107.7	32.8	128.3	31.1	129.9	10.9	20	400–430
	B3 component (third group; transitional direction)										
7	Gwest1 (Horseleg Mtn)	4/5	320/78	239.2	16.1	247.7	−5.3	414.9	4.5	20–200	500–640
8	Gwest2 (Horseleg Mtn)	4/4	319/70	242.8	46.6	276.5	5.3	23.7	19.3	20–300	400–590

and has a lower unblocking temperature (<430 °C) than the B1 component. Directions of the B2 component before tilt correction are to the east-to-southeast with moderate to high inclinations. After tilt correction, the B2 direction of these two sites moves toward the in-situ site-mean direction of the B1 component, possibly suggesting a pre-folding age of magnetization (Fig. 8e and f). Sites 6 (eastern flank of the Horseleg Mountain anticline) and 9 (northeastern segment of the Helena thrust sheet) have map patterns that suggest more than two events of deformation (see discussion of out-of-sequence thrusting in Section 3.2 on timing of deformation), but a more significant number of cores is needed to corroborate this suggestion. The third group includes two sites on the northwestern flank of the Horseleg Mountain anticline, where the directions of the B3 component are to the southwest with moderate downward inclinations (Fig. 6c). After tilt correction, the direction remains to the southwest but with very shallow inclinations. We interpret the B3 direction as a possible composite direction of the B1 and C1 components. The south-to-southeast and downward direction of the B1 component corresponds to the well-defined late Paleozoic event of remagnetization.

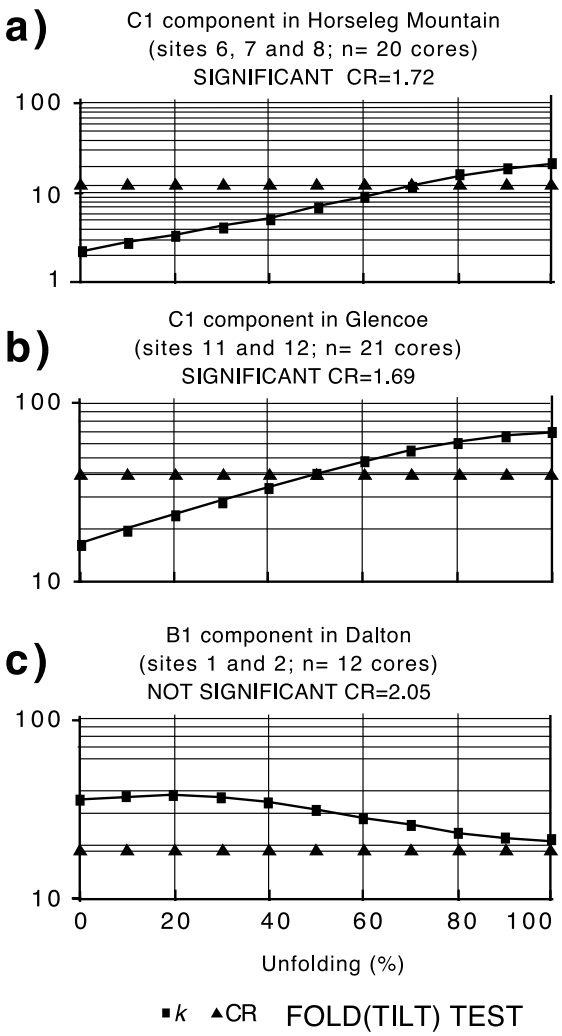

Fig. 7. Results of local incremental inclination-only fold tests for the C1 component ((a) and (b)) and B1 component (c). These diagrams plot k (squares, an estimate of the degree of clustering of inclination data on a sphere) and CR (triangles, a critical ratio above which k values become significant at the 95% confidence level) (McElhinny, 1964) versus percent of unfolding. (a) and (b) show a positive fold(tilt) test for component C1; (c) is a negative fold(tilt) test with a decrease of k during incremental unfolding.

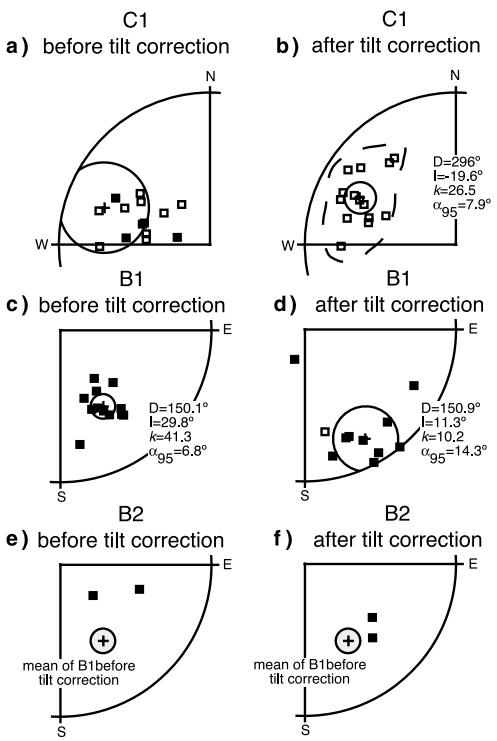

Fig. 8. Equal-area plots of site-mean directions for components C1, B1, and B2. Open (solid) symbols are points in upper (lower) hemisphere. Paleomagnetic directions of C1 component show a good cluster after tilt correction (b); the ellipsoidal distribution of C1 directions suggests deviation of declinations by rotations. In contrast, the directions of component B1 have a good cluster before tilt correction (c). Note the closer similarity of components B2 after tilt correction (sites 6 and 9) to the mean direction of the B1 component (see text for discussion).

6.4. Comparison of structural-domain mean and reference declinations

The ellipsoidal distribution of site-mean (C1) declinations (Fig. 8b) is expected because the sites are located in structures with deviations from the regional structural strike and may have experienced (sub)vertical-axis rotations. The lack of sites in structures striking parallel to the regional trend and the irregular distribution of sites within selected structures limit the usefulness of the C1 mean direction as a local reference declination. An alternative is to calculate a reference declination using the APWP of Laurentia for Paleozoic time.

The general agreement of the C1 site-mean directions (296°/ − 19.6°) with other established Upper Ordovician directions suggests that the characteristic magnetization was acquired shortly after deposition. A precise age has not been reported for rocks of the Greensport Formation; however, a late Middle to early Late Ordovician age (early Mohawkian) is constrained by conodonts from the underlying carbonate unit (Hall et al., 1986) and radiometric ages from K-bentonites in the overlying unit (Kunk and Sutter, 1984; Kolata et al., 1996). Paleomagnetic poles for the Ordovician have been calculated from Lower Ordovician and uppermost Ordovician units (see Van der Voo (1990) and Mac Niocaill et al. (1997) for source of data). A reference direction (309°/ − 28°) for the thrust belt in Georgia and Alabama was determined using the Middle–Late Ordovician paleopole position of Laurentia calculated by Mac Niocaill et al. (1997) (paleopole = 21°N, 148°E). The reference paleomagnetic direction (309°/ − 28°) is very similar to the tilt-corrected site-mean C1 direction of site 0 (310°/ − 25°; Table 1; from Morrison and Ellwood, 1986), and the mean C1 direction from this study (296°/ − 19.6°), supporting an age of magnetization no younger than latest Ordovician. Site 0 is located in the Kingston thrust sheet (Fig. 3), a structure that follows the regional strike of the thrust belt in northwestern Georgia.

Opposing senses of rotation and slight flattening are observed in different structural domains in the Clinchport–

Table 2
Differences of declination/inclination between structural domains (ΔDsd° and ΔIsd°) in the Clinchport–Horseleg thrust sheet (CHTS, Georgia) and the Helena thrust sheet (HTS, Alabama). Site = list of sites within each structural domain, n = number of cores used in calculation of the tilt-corrected mean declination/inclination (Dsd/Isd) of the C1 component for each structural domain. The confidence limits for structural domain declinations (Dsd error° and Isd error°) and the difference of declinations and inclinations (ΔDsd error° and ΔIsd error°) follow the criteria given by Demarest (1983)

Structural domain	Site	n	Dsd°	Dsd error(°)	ΔDsd°	ΔDsd error(°)	Isd°	Isd error(°)	ΔIsd°	ΔIsd error(°)
Between assymetrical folds in the Clinchport thrust sheet (Georgia)										
Southeast-plunging fold	2	7	269.2	13.4			−15.5	12.9		
North-striking fold	3, 4	12	295.1	11.0			−15.7	10.6		
					25.9	17.3			−0.2	16.7
Between southeast- and and northeast-plunging folds in CHTS (Georgia)										
Southeast-plunging fold	2	7	269.2	13.4			−15.5	12.9		
Northeast-plunging fold	6	12	324.1	7.8			−20	7.3		
					54.9	15.5			4.5	14.8
Between northeastern and southwestern segments of the HTS (Alabama)										
Northeastern segment	9	10	320.6	4.2			−20.2	3.9		
Southwestern segment	13–16	13	300.1	9.1			−21	8.5		
					20.5	10.0			0.8	9.4
Between the southwestern segment of the HTS and sites near the transverse fault										
Sites near the transverse fault	10–12	27	288.5	4.3			−17.2	4.1		
Southwestern segment	13–16	13	300.1	9.1			−21	8.5		
					11.6	10.1			3.8	9.4

Horseleg thrust sheet (CHTS) and in the Helena thrust sheet (HTS) (Table 2; Fig. 9a and b). The southeast-plunging fold (site 2) and north-striking fold (sites 3 and 4) in the northern CHTS have counter-clockwise (CCW) rotations with greater magnitude of rotation in southeast-plunging folds. In contrast, the northeast-plunging fold (site 6) in the southern CHTS shows clockwise (CW) rotations. A significant difference between declinations (in contrast to similarity in inclinations) exists between southeast- and northeast-plunging folds (ΔDsd = 54.9° ± 15.5°; ΔIsd = 4.5° ± 14.8°; Table 2; Fig. 9a). The declination of site 9 in the northeastern segment of the HTS indicates CW rotations. The sites near the transverse fault (sites 10–12) as well as the sites in the southwestern segment (sites 13–16) indicate CCW sense of rotation, with greater magnitudes in sites near the transverse fault. The mean declination and cones of 95% confidence between northeastern and southwestern segments of the HTS (ΔDsd = 20.5° ± 10°) plot apart and on opposite sides of the reference paleomagnetic direction (Table 2; Fig. 9b).

Although both the CHTS and the HTS have contrasting internal structural domains, a moderate to weak correlation is recognized between variation of paleomagnetic declinations and structural strike domains (strike test of Schwartz and Van der Voo, 1983) (Table 3; Fig. 9c and d). An excellent correlation (slope = 1) is expected in curved orogenic belts that were originally straight (e.g. the Cantabria–Asturias arc; Weil et al., 2000); moderate correlations have been interpreted for some primary curved belts (e.g. Schwartz and Van der Voo, 1984; Stamatakos and Hirt, 1994). A total absence of declination variation may indicate absence of rotations or magnetization acquisition after rotation. Local rotations and a moderate to weak correlation between strike and declination deviations may be related to more local effects, such as detachment level

Table 3
Calculation of declination deviations (D–Dr) and strike deviations (S–Sr) for the strike test of Schwartz and Van der Voo (1983). The reference strike (Sr) and reference declination (Dr) are given in Fig. 9c and d. Declination error is shown for sites with $N > 2$ (see Table 1)

	Site	S°	S–Sr(°)	D°	D–Dr(°)	D error (°)
0	Ringgold gap	15	2	310	11	8.8
2	C (Dalton)	145	−48	269.2	−29.8	13.4
3	Deast (Hamilton Mtn)	199	6	295.8	−3.2	12.5
4	Dwest1 (Hamilton Mtn)	6	−7	291.3	−7.7	
6	Geast (Horseleg Mtn)	54	41	324.1	25.1	7.8
9	Canon gap (N. Helena)	115	55	320.6	25.6	4.2
10	Alexander gap	111	51	287	−8	13
11	E. Glencoe	104	44	294.6	−0.4	3.9
12	W. Glencoe	340	−80	283.4	−11.6	5.1
13	Greensport gap1	73	13	308.7	13.7	12.7
14	Greensport gap2	80	20	292.1	−2.9	9.1
15	US231 gap-1	49	−11	284	−11	
16	US231 gap-2	55	−5	294.7	−0.3	3.8

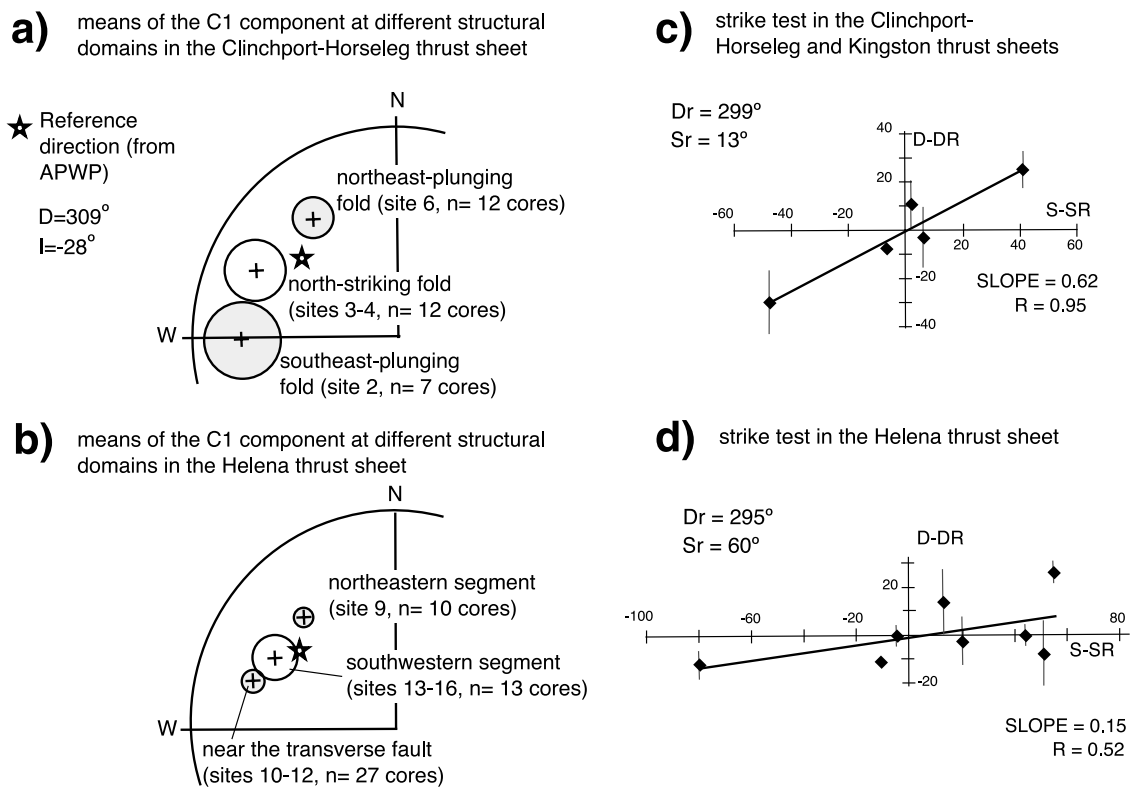

Fig. 9. Equal area plots ((a) and (b)) showing structural-domain-mean directions for the C1 component (see Table 2) and the reference paleomagnetic direction for Middle–Late Ordovician time. See text for discussion of rotations. Strike tests ((c) and (d)) of Schwartz and Van der Voo (1983) consist of declination deviations (D–Dr) from a reference declination (Dr) of site means of C1 component plotted against strike deviations (S–Sr) from a reference strike (Sr). Data from Table 3. Each diagram shows a linear regression line, slope, and correlation coefficient (R). Dr values were chosen so the regression line crosses the origin of the plot; Sr is the strike of cross-sections X–X′ (c) and Y–Y′ (d). These two diagrams show a moderate (c) to a very poor (d) correlation of these two parameters.

stratigraphy or a complex three-dimensional geometry of the thrust belt (i.e. oblique/lateral/frontal ramps, transverse faults, several detachment levels); we believe this to be applicable to our study. Consequently, the local curvature of structures in the HTS and CHTS may be the result of rotations about (sub)vertical axes (e.g. Apotria et al., 1992).

7. Discussion

Our study focuses on local structures, the strike deviations of which are not transmitted to either leading or trailing thrust sheets, but they are within transverse zones. Consequently, internal deviations within thrust sheets are related to changes in internal configuration of thrust sheets in palinspastic position, such as stratigraphic pinch outs and three-dimensional trajectory of ramp/flat surfaces, and this internal configuration of thrust sheets is primarily controlled by sub-décollement basement faults (see Section 3.2).

Differential slip along the Clinchport and Horseleg faults, as indicated by the concave-to-the hinterland restored geometry of the strike-parallel line X–X′ (Figs. 3 and 10), is related to the contrasting rheologies (or rock strength) between detachment levels in lateral ramps and to geometry of lateral ramps. In map view, the two sets of studied plunging folds within the Clinchport–Horseleg thrust sheet are in hanging-wall lateral ramps. Deviations in structural strike of the plunging folds record the deflection of the regional transport direction at lateral structures (i.e. out-of-plane deformation; Apotria et al., 1992; Wilkerson et al., 1992; Apotria, 1995) and accommodate the differences of displacement between the lower and upper detachment flats. The southward change of detachment level along the Clinchport fault from a weak layer to a stiff layer is interpreted to cause differential slip and CCW rotations (Fig. 10, Dalton area). In the Horseleg Mountain area, the northward abrupt change in detachment level from unit 1 to units 2 and 3 causes differential slip and CW rotations.

Kinematic models of deformation at oblique/lateral ramps predict that deflection of tectonic transport trajectory increases with dip of the lateral/oblique ramp (Apotria et al., 1992). Deviations in fold axes and paleomagnetic declinations in the Clinchport lateral ramp support this interpretation. The relative magnitude of CCW rotations is greater in structures that formed at the hanging-wall lateral ramp cutoff (i.e. south-southeast-plunging anticlines, sites 1 and 2) than in structures that formed at greater distance from the lateral ramp (north-trending folds, sites 3–5) ($\Delta D\mathrm{sd} = 25.9° \pm 17.3°$; Table 2). The Horseleg lateral ramps cut at higher angles to bedding (30–40°) than the

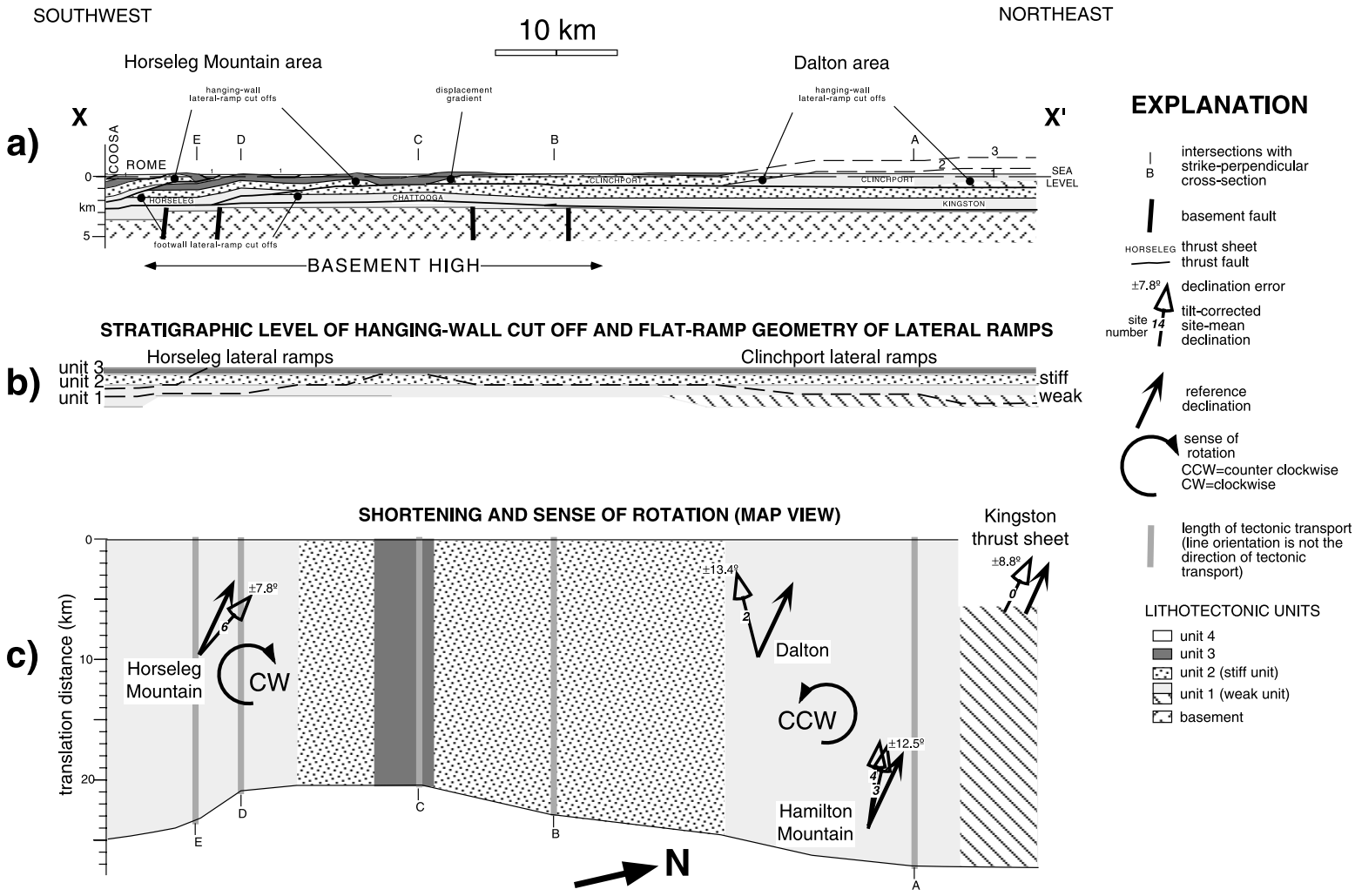

Fig. 10. (a) Cross-section showing along-strike changes of thickness and stratigraphic units in hanging-wall lateral ramp cut-offs in deformed stage (see Fig. 2 for location of line X–X′). Plunging folds are on the upper detachment flat (e.g. Dalton area) and on the lateral ramp (e.g. Horseleg Mountain area). (b) Cross-section showing along-strike changes of thickness and stratigraphic units at hanging-wall lateral ramps. Note the difference in flat dimensions and ramp-flat angle between Clinchport and Horseleg lateral ramps. (c) Map showing relationship of differential shortening and (sub)vertical-axis rotations to the geometry of lateral ramps and lithologies at detachment levels. Note the linear match of strike-perpendicular cross-sections A–E between cross-sections and map view. Calculation of translation distance is explained in Fig. 3. Paleomagnetic declination in the Kingston thrust sheet (Morrison and Ellwood, 1986) is shown in the upper right corner.

Clinchport lateral ramps (8–15°); the deviation in strike of fold axes within the Horseleg Mountain thrust sheet (>36°) is greater than the observed deviations in strike of fold axes in the Clinchport thrust sheet (<30°) (Fig. 3). However, the magnitudes of deviations of strike and rotations of paleomagnetic declination have a moderate correlation (Table 3; Fig. 9c). In addition, the observed strike deviations (i.e. deflection out of transport plane) are much higher than those predicted by kinematic models (<3° in Dalton area; <8° in Horseleg Mountain area; values calculated from fig. 8 in Apotria et al., 1992). The discrepancy in magnitudes among paleomagnetic declinations, strike of structures, and predicted deflection indicate that variables, such as mechanical properties of rocks at different detachment levels and weight of overburden (e.g. Wilkerson et al., 1992), also play a role in rotations and kinematics of plunging folds at lateral structures.

Location and the contrasting geometry of the Clinchport and Horseleg lateral ramps coincide with the boundaries of a shallow basement domain (Fig. 10). This shallow domain of the top of basement is bounded on the north by a transverse fault and a gentle northeast deepening of the top of basement, and on the south by a complex system of transverse faults and an abrupt southwest deepening of the top of basement.

The contrasting geometry and rotations within the Helena thrust sheet (HTS) are the result of the different history of emplacement of the northeastern and southwestern segments across the Birmingham graben (BG), as well as of the hanging-wall oblique ramp cut-off of the detachment surface in the northeastern segment. The HTS palinspastically restores almost completely on the southeast shoulder of the BG, and the leading trace of the HTS is broken above the transverse basement fault (Fig. 11a). During initial northwestward emplacement of the entire HTS, the underlying transverse basement fault partitioned the kinematics of the two segments because of the sub-décollement structural relief of basement and footwall deformation. The northeastern segment, a hanging-wall oblique ramp, moved over the undeformed Peavine oblique/frontal footwall ramp. CW rotations and brittle deformation (Graham, 1999) in the northeastern segment are the result of differential slip caused by contrasting rheologies of beds at the hanging-wall oblique ramp cut-off and reverse movement along the transverse fault. In contrast, the southwestern segment of the HTS was transported passively down within the BG following the trailing ramp (Dunaway Mountain thrust sheet) of a mushwad structure (Thomas, 2001), and the HTS was draped over the basement transverse fault and Peavine footwall transverse fault (Fig. 11b). Tectonic thickening of unit 1 near the transverse fault favored differential slip and CCW rotation in the southwestern segment. As northwestward translation continued, the southwestern segment of the HTS broke back as an out-of-sequence structure (Thomas, 2001), and translation over a footwall oblique ramp in unit 4 bent the northeastern segment of the HTS to its present configuration (Fig. 11c). Interference folds and accommodation fault structures in the southwestern segment formed at the intersection between the Dunaway Mountain frontal ramp and the transverse fault; these structures record an increase of CCW rotation near the transverse zone (Table 2; Fig. 9b).

Kinematic and mechanical models have predicted hanging-wall shortening, such as interference folds and accommodation fault structures, in the foreland intersection between frontal and lateral structures (Apotria et al., 1992; Stewart, 1993). In contrast, the northeastern segment moved over a second footwall oblique ramp within the Peavine footwall; CW rotations might have continued as a result of Peavine footwall geometry and differential slip. A similar example of vertical-axis rotations across a thin-skinned transverse fault has been documented in the foreland thrust belt of Papua New Guinea (Weiler and Coe, 1997), where the transverse fault is aligned above a lower-plate fault.

8. Conclusions

Plunging folds and faults in intermediate imbricate faults of the southernmost Appalachians have irregular orientations that contrast with the linear northeasterly strike of leading structures. We investigate the causes of deviations in structural strike of local structures within transverse zones using an iterative comparison of structural cross-sections, sub-décollement basement structures, and pre-folding paleomagnetic declinations from Upper Ordovician clastic rocks.

Different structural domains of the Clinchport–Horseleg thrust sheet (CHTS) and the Helena thrust sheet (HTS) yield opposite senses of rotations. In the CHTS from north to south, the Clinchport fault cuts gradually up section from a weak to a stiff unit forming southeast-plunging folds. In the southern extreme of the CHTS, from south to north, blind faults cut abruptly up section from a weak to a stiff unit forming northeast-plunging folds. The mechanisms to produce hanging-wall plunging folds, variations in the magnitude of shortening, and rotations are interpreted as a combination of displacement gradient and the presence of lateral ramps. Counter clockwise (CCW) and CW rotations in northern and southern folds, respectively, indeed document the sense of rotations predicted for hanging-wall lateral-ramp plunging folds. The northeasterly strike of the southwestern segment of HTS changes across a transverse fault to an easterly strike in the northeastern segment of the Helena fault. In the northeastern segment, the fault cuts up section from a weak to a stiff unit (oblique ramp) in the hanging wall. CW rotations and brittle deformation documented in the northeastern segment support the interpretation of rotations in response to contrasting rheologies within the hanging-wall oblique ramp cutoff. In contrast, the southwestern segment rotated in the opposite sense (CCW) as it moved down within a

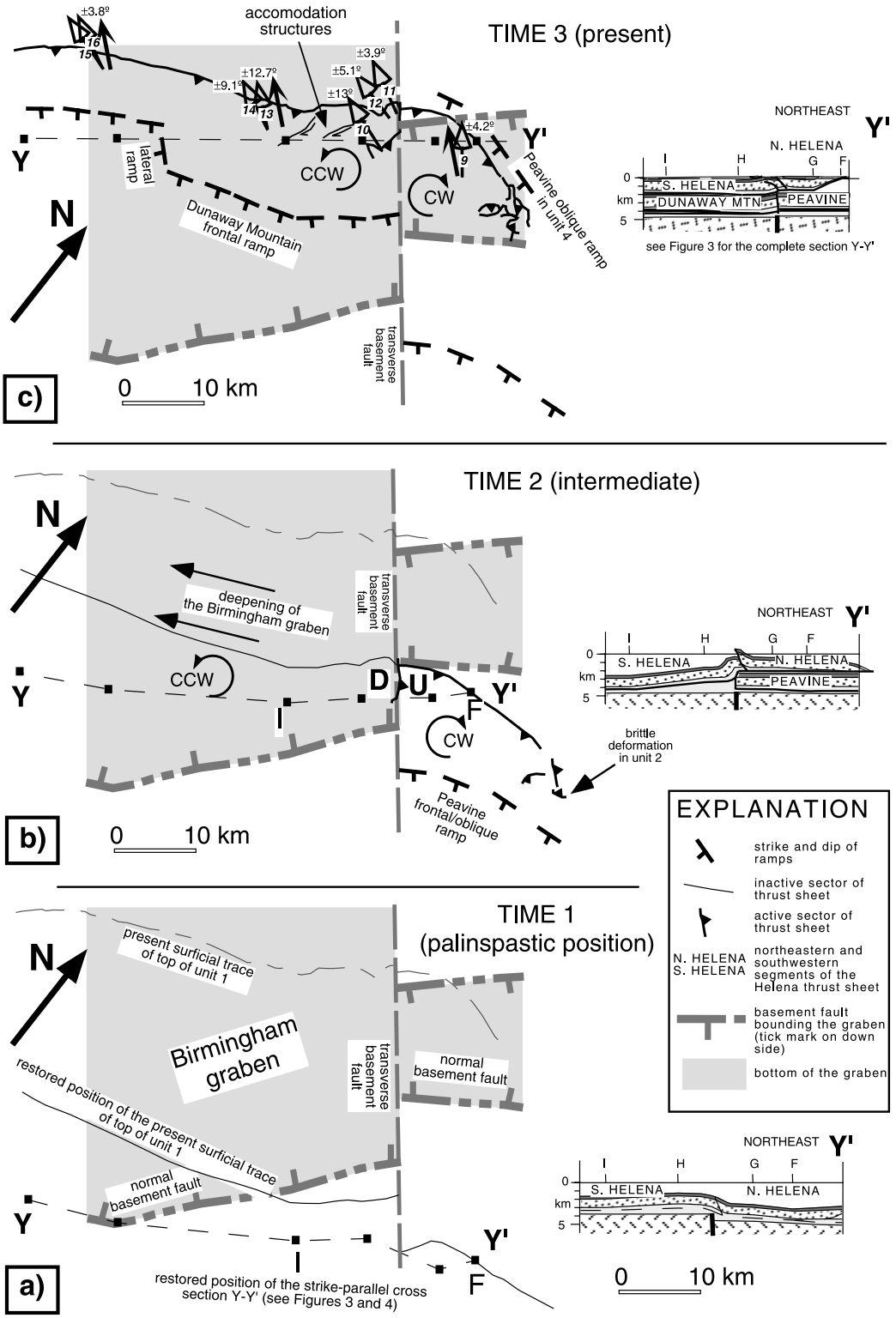

Fig. 11. Map view and strike-parallel cross-sections showing the northwestward emplacement of the Helena thrust sheet (HTS) over the sub-décollement basement graben structure at three intervals of time (map view), and the relationship of the position of line Y–Y′ to the subdetachment basement relief and footwall geometry (cross-sections). Abbreviations and symbols as in Fig. 10. See text for discussion of rotations.

wide, deep graben. Footwall ramp geometry and deformation also controlled hanging-wall shortening and rotations.

In short, rotations in the CHTS and HTS occurred within transverse zones as the thrust sheets moved over oblique/lateral ramps with contrasting rock strengths at lower and upper detachment levels, over transverse basement faults that separate contrasting elevations of basement in the

Birmingham graben, and at intersections between frontal ramps and lateral/oblique structures.

Because of the local causes of rotations in transverse faults and plunging folds, as reported in this paper, paleomagnetic sampling in such lateral structures is needed to constrain the effects of local vertical-axis rotations in the kinematics of single thrust sheets. Furthermore, documentation of vertical-axis rotations allows a more precise restoration of pre-existing structures (e.g. cleavage, fractures, lineaments) and paleocurrent directional indicators collected along transverse faults and in plunging folds. In regional kinematics analysis of curved orogenic belts (large-scale salients and recesses), however, paleomagnetic samples from lateral structures must be used with caution to separate a potential strong local effect on vertical-axis rotations from any possible regional rotations.

Acknowledgements

This research was supported by a grant from the Geological Society of America and a Dissertation Enhancement Award from the University of Kentucky Graduate School. Acknowledgment is made to the Donors of the Petroleum Research Fund (33390), administered by the American Chemical Society, for partial support of this research. GB acknowledges Arlo B. Weil and Josep Parés for their guidance during the paleomagnetic analysis at the University of Michigan; Brian Cook and Brent Garry for their help during field work; Seismic Exchange Inc. for access to one seismic line in Georgia, and Vulcan Materials for access to quarries. We appreciate the comments of John Geissman, Camilo Montes, Ken Kodama and Kevin Smart, which improved the content of this manuscript.

References

Allerton, S., 1998. Geometry and kinematics of vertical axis rotations in fold and thrust belts. Tectonophysics 299, 15–30.

Apotria, T.G., 1995. Thrust sheet rotation and out-of-plane strains associated with oblique ramps: an example from the Wyoming salient, USA. Journal of Structural Geology 17, 647–662.

Apotria, T.G., Snedden, W.T., Spang, J.H., Wiltschko, D.V., 1992. Kinematic models of deformation at an oblique ramp. In: McClay, K.R., (Ed.), Thrust Tectonics, Chapman & Hall, pp. 141–154.

Bayona, G., Thomas, W.A., 2001. Implication of a palinspastic map for the stratigraphic and tectonic framework of the Alabama–Georgia Appalachian thrust belt. Geological Society of America Abstract with Programs 33 (2), 18.

Bayona, G., 2003. Controls on Middle to Late Ordovician synorogenic deposition in the southeastern corner of Laurentia. Ph.D. dissertation, University of Kentucky.

Boyer, S.E., Elliott, D., 1982. Thrust systems. American Association of Petroleum Geologists Bulletin 66, 1196–1230.

Carter, B.D., Chowns, T.M., 1986. Stratigraphical and environmental relationships of Middle and Upper Ordovician rocks in northwestern Georgia and northeastern Alabama. In: Benson, D.J., Stock, C.W. (Eds.), Depositional History of the Middle Ordovician of the Alabama Appalachians. 23rd Annual Field Trip Guidebook, Alabama Geological Society, pp. 33–50.

Chowns, T.M., Carter, B.D., 1983. Middle Ordovician section along Mount Alto Road at southwest end of Horseleg Mountain. In: Chowns, T.M. (Ed.), Geology of Paleozoic rocks in the Vicinity of Rome, Georgia. 18th Annual Field Trip Guidebook, Georgia Geological Society, pp. 70–73.

Coleman, J.L. Jr., 1988. Geology of the Rising Fawn CSD. In: Coleman, J.L. Jr., Groshong, R.H. Jr., Rheams, K.F., Neathery, T.L., Rheams, L.J. (Eds.), 25th Annual Field Trip Guidebook, Alabama Geological Society, pp. 12–40.

Cressler, C.W., 1970. Geology and ground-water resources of Floyd and Polk Counties, Georgia. Georgia Geological Society Information Circular 39, 95pp.

Cressler, C.W., 1974. Geology and ground-water resources of Gordon, Whitfield, and Murray Counties, Georgia. Georgia Geological Society Information Circular 47, 35pp.

Demarest, H.H. Jr, 1983. Error analysis for the determination of tectonic rotation from paleomagnetic data. Journal of Geophysical Reserach 88, 4321–4328.

Drahovzal, J.A., Neathery, T.L., 1971. Middle and Upper Ordovician stratigraphy of the Alabama Appalachians. In: Drahovzal, J.A., Neathery, T.L. (Eds.), The Middle and Upper Ordovician of the Alabama Appalachians. 9th Annual Field Trip Guidebook, Alabama Geological Society, pp. 1–62.

Eldredge, S., Van der Voo, R., 1988. Paleomagnetic study of thrust sheet rotations in the Helena and Wyoming salients of the northern Rocky Mountains. In: Schmidt, C., Perry, W. (Eds.), Interaction of the Rocky Mountains Foreland and the Cordilleran Thrust Belt. Geological Society of America Memoir 171, pp. 319–332.

Fisher, R.A., 1953. Dispersion on a sphere. Proceedings of the Royal Society of London Series A 217, 295–305.

Garry, W.B., 2001. Stratigraphy and structure of the Dunaway Mountain thrust sheet revealed through geologic mapping and interpretation of the Ashville 7.5 minute quadrangle, Alabama. M.S. thesis, University of Kentucky.

Graham, G.B., 1999. Geometry and kinematics of two juxtaposed lateral ramps, southern Appalachian Thrust belt in northeastern Alabama. M.S. thesis, University of Kentucky.

Grubbs, K.L., Van der Voo, R., 1976. Structural deformation of the Idaho–Wyoming overthrust belt (USA), as determined by Triassic paleomagnetism. Tectonophysics 33, 321–336.

Hall, J.C., Bergström, S.M., Schmidt, M.A., 1986. Conodont biostratigraphy of the Middle Ordovician Chickamauga Group and related strata of the Alabama Appalachians. In: Benson, D.J., Stock, C.W. (Eds.), Depositional History of the Middle Ordovician of the Alabama Appalachians. 23rd Annual Field Trip Guidebook, Alabama Geological Society, pp. 61–80.

Hodych, J.P., Patzold, R.R., Buchan, K.L., 1985. Chemical remanent magnetization due to deep-burial diagenesis in oolitic hematite-bearing ironstones of Alabama. Physics of the Earth and Planetary Interiors 37, 261–284.

Kent, D.V., 1988. Further paleomagnetic evidence for oroclinal rotation in the central folded Appalachians from the Bloomsburg and the Mauch Chunk Formations. Tectonics 7, 749–759.

Kolata, D.R., Huff, W.D., Bergström, S.M., 1996. Ordovician K-bentonites of eastern North America. Geological Society of America Special Paper 313, 1–69.

Kunk, M.J., Sutter, J.F, 1984. $^{40}Ar/^{39}Ar$ age spectrum dating of biotite from Middle Ordovician bentonites, eastern North America. In: Brunton, D.L. (Ed.), Aspect of the Ordovician System. Palaeontological Contributions of the University of Oslo 295, pp. 11–22.

McCaig, A.M., McClelland, E., 1992. Paleomagnetic techniques applied to thrust belts. In: McClay, K.R., (Ed.), Thrust Tectonics, pp. 209–216.

McElhinny, M.W., 1964. Statistical significance of the fold test in paleomagnetism. Geophysical Journal of the Royal Astronomical Society 8, 338–340.

McFadden, P.L., Reid, A.B., 1982. Analysis of paleomagnetic inclination data. Geophysical Journal of the Royal Astronomical Society 69, 307–319.

Mac Niocaill, C.M., van der Pluijm, B.A., Van der Voo, R., 1997. Ordovician Paleogeography and the evolution of the Iapetus ocean. Geology 25, 159–162.

Montgomery, J.M., Jr., 1993. The origin of structural curvature in the northern part of the Wyoming–Idaho thrust belt, Wyoming–Idaho. M.S. thesis, University of Kentucky.

Morrison, J., Ellwood, B.B., 1986. Paleomagnetism of Silurian–Ordovician sediments from the Valley and Ridge province, northwest Georgia. Geophysical Research Letters 13, 189–192.

Osborne, E.W., Szabo, M.W., Neathery, T.L., Jr., Copeland, C.W., 1988. Geologic map of Alabama, northeast sheet. Alabama Geological Survey Special Map 220, scale 1:250,000.

Paulsen, T., Marshak, S., 1999. Origin of the Uinta recess, Sevier fold-thrust belt, Utah: influence of basin architecture of fold-thrust belt geometry. Tectonophysics 312, 203–216.

Perroud, H., Van der Voo, R., 1984. Secondary magnetizations from the Clinto-type iron ores of the Silurian Red Mountain Formation, Alabama. Earth and Planetary Sciences Letters 67, 391–399.

Rankin, D.W., 1976. Appalachian salients and recesses; late Precambrian continental breakup and the opening of the Iapetus Ocean. Journal of Geophysical Research 81, 5605–5619.

Schwartz, S.Y., Van der Voo, R., 1983. Paleomagnetic evaluation of the orocline hypothesis in the Central and Southern Appalachians. Geophysical Research Letters 10, 505–508.

Schwartz, S.Y., Van der Voo, R., 1984. Paleomagnetic study of thrust sheet rotation during foreland impingement in the Wyoming–Idaho over-thrust belt. Journal of Geophysical Research 89, 10077–10086.

Stamatakos, J., Hirt, A.M., 1994. Paleomagnetic considerations of the development of the Pennsylvanian salient in the central Appalachians. Tectonophysics 231, 237–255.

Stamatakos, J., Kodama, K.P., 1991a. Flexural flow folding and the paleomagnetic fold test: an example of strain reorientation of remanence in the Mauch Chunk Formation. Tectonics 10, 807–817.

Stamatakos, J., Kodama, K.P., 1991b. The effect of grain-scale deformation on the Bloomsburg Formation pole. Journal of Geophysical Research 96, 17919–17933.

Stamatakos, J., Hirt, A.M., Lowrie, W., 1996. The age and timing of folding in the central Appalachians from paleomagnetic results. Geological Society of America Bulletin 108, 815–829.

Stewart, S.A., 1993. Fold interference structures in thrust systems. Tectonophysics 225, 449–456.

Thomas, W.A., 1977. Evolution of Appalachian–Ouachita salients and recesses from reentrants and promontories in the continental margin. American Journal of Science 277, 1233–1278.

Thomas, W.A., 1985. Northern Alabama sections. In: Woodward, N.B. (Ed.),Valley and Ridge Thrust Belt: Balanced Structural Sections, Pennsylvania to Alabama (Appalachian Basin Industrial Associates). University of Tennessee Department of Geological Sciences Studies in Geology 12, pp. 54–61.

Thomas, W.A., 1990. Controls on locations of transverse zones in thrust belts. Eclogae Geologicae Helvetica 83, 727–744.

Thomas, W.A., 2001. Mushwad: ductile duplex in the Appalachian thrust belt in Alabama. American Association of Petroleum Geologists Bulletin 85, 1847–1869.

Thomas, W.A., Bayona, G., 2001. Three-dimensional palinspastic restoration of the unmetamorphosed Appalachian thrust belt in Alabama and Georgia. Geological Society of America Abstract with Programs 33 (2), 5.

Thomas, W.A., Bayona, G., 2002. Palinspastic restoration of the Anniston Transverse Zone in the Appalachians thrust belt, Alabama. Journal of Structural Geology 24, 797–826.

Thomas, W.A., Astini, R.A., Osborne, W.E., Bayona, G., 2000. Tectonic framework of deposition of the Conasauga Formation. In: Osborne, W.E., Thomas, W.A., Astini, R.A. (Eds.), The Conasauga Formation and Equivalent Units in the Appalachian Thrust Belt in Alabama. 37th Annual Field Trip Guidebook, Alabama Geological Society, pp. 19–40.

Van der Voo, R., 1990. Phanerozoic paleomagnetic poles from Europe and North America and comparisons with continental reconstructions. Reviews of Geophysics 28, 167–206.

Watts, D.R., Van der Voo, R., 1979. Paleomagnetic results from the Ordovician Moccasin, Bays, and Chapman Ridge Formations of the Valley and Ridge province, Eastern Tennessee. Journal of Geophysics Research 84, 645–655.

Weil, A.B., Van der Voo, R., van der Pluijm, B.A., Parés, J.M., 2000. The formation of an orocline by multiphase deformation: a paleomagnetic investigation of the Cantabria–Asturias Arc (northern Spain). Journal of Structural Geology 22, 735–756.

Weiler, P.D., Coe, R.S., 1997. Paleomagnetic evidence for rapid vertical-axis rotations during thrusting in an active collision zone, northeastern Papua New Guinea. Tectonics 16, 537–550.

Wilkerson, M.S., Marshak, S., Bosworth, W., 1992. Computerized tomographic analysis of displacement trajectories and three-dimensional fold geometry above oblique thrust ramps. Geology 20, 439–442.

Wilkerson, M.S., Apotria, T., Farid, T., 2002. Interpreting the geologic map expression of contractional fault-related fold terminations: lateral/oblique ramps versus displacement gradients. Journal of Structural Geology 24, 647–662.

Zijderveld, J.D.A., 1967. A.C. demagnetization of rocks: analysis of results. In: Collison, D.W., Creer, K.M., Runcorn, S.K. (Eds.), Methods of Paleomagnetism, Elsevier Science, pp. 254–286.